THE ASTROPHYSICAL JOURNAL SUPPLEMENT SERIES, 80:645–681, 1992 June

THE X-RAY SPECTRA OF GALAXIES. I. SPECTRAL FITS OF INDIVIDUAL GALAXIES AND X-RAY COLORS

D.-W. KIM AND G. FABBIANO
Harvard-Smithsonian Center for Astrophysics, 60 Garden Street, Cambridge, MA 02138
AND
G. TRINCHIERI
Osservatorio Astrofisico di Arcetri and Harvard-Smithsonian Center for Astrophysics, 60 Garden Street, Cambridge, MA 02138
Received 1991 June 12; accepted 1991 October 30;

ABSTRACT

We have systematically investigated the X-ray spectra of normal galaxies, by using the Imaging Proportional Counter (IPC) data in the *Einstein* data bank. In addition to the standard model fitting technique, we introduce X-ray colors in order to extract spectral information from the fainter X-ray sources. We present spectral parameters for 43 galaxies and X-ray colors for 127 galaxies.

Subject heading: X-rays: galaxies

1. INTRODUCTION

Since the launch of the *Einstein* satellite in 1978 (Giacconi et al. 1979), X-ray observations have added important information to our knowledge of normal galaxies (see Fabbiano 1989 for a review). Most of the work done so far, however, has been concentrated on the analysis of imaging data. Spectral parameters [i.e., hydrogen absorption column density and emission temperature (or power-law index)] can be extracted for sources observed with the Imaging Proportional Counter (IPC), but have been published only for a limited number of normal galaxies (for six elliptical galaxies, Trinchieri, Fabbiano, & Canizares 1986; for 13 spiral galaxies, Fabbiano & Trinchieri 1987; for the bulge of M31, Fabbiano, Trinchieri, & Van Speybroeck 1987; for N1399, Killeen & Bicknell 1988; for M33, Trinchieri, Fabbiano, & Peres 1988; for M81, Fabbiano 1988a; for M101, Trinchieri, Fabbiano, & Romaine 1990; and for the starburst galaxies NGC 253 and M82, Fabbiano 1988b). Forman, Jones & Tucker (1985) gave temperature ranges for eight early-type galaxies, but not fitting N_H, for which they assumed the Galactic line-of-sight value. An extensive IPC spectral survey of Seyfert galaxies has been recently published (Kruper, Urry, & Canizares 1990, hereafter KUC). The X-ray emission of these galaxies is dominated by their active nuclear source (AGN).

Spectral information is essential for a more concrete understanding of the nature of the X-ray sources and of the emission mechanisms in galaxies. Because different types of galaxies are likely to consist of different mixtures of X-ray emitting components, which may have different spectral characteristics, searching for differences in their spectral properties may help us identifying the dominant component for a given class of galaxies. We have performed a systematic spectral analysis of all the galaxies in the catalog of Fabbiano, Kim, & Trinchieri (1992, hereafter Paper I) and we present the results in this paper. For galaxies detected with high signal-to-noise ratio we present the results of a two-parameter χ^2 fit of emission models to the data. However, most galaxies observed with the *Einstein* Observatory IPC do not have enough counts for us to apply this model fitting technique. To extract X-ray spectral information from faint sources, we have introduced and calibrated two X-ray colors so that two important parameters—emission temperature (or power-law index) and hydrogen column density responsible for the low-energy cutoff—can be determined. X-ray colors, although with a different definition from ours, have been used by Cordova et al. (1990) to find very soft X-ray sources.

Galaxies from Paper I observed with the *Einstein* IPC are included for this spectral study if detected with more than 30 net counts. Galaxies which have ambiguous sources (i.e., the X-ray emission could be due to interlopers) or were partly hidden by the detector supporting structure are excluded. These galaxies are listed in Tables 3 and 6 of Paper I. We describe the standard model fitting technique and present the results in § 2. We describe the X-ray colors and present the results in § 3. We include notes on individual galaxies in § 4. In a forthcoming paper, we will discuss the average spectral properties of different types of galaxies and their implications on the X-ray emission mechanisms (Kim, Fabbiano, & Trinchieri 1992, hereafter Paper III).

2. STANDARD MODEL FITTING

2.1. *Analysis and Results*

In the standard model fitting method [for example, see *Einstein* Revised User's Manual (Harris 1984, hereafter RUM)], a two-parameter model (e.g., kT and N_H for a bremsstrahlung spectrum with low-energy cutoff; α and N_H for a power-law spectrum with low-energy cutoff) is convolved with the instrumental response of the *Einstein* IPC for a range of spectral parameters, and then compared with the observed distribution of counts in the IPC pulse height (PH) channels using the minimum χ^2 technique. We restricted our fits to PH channels corresponding to energies in the range of ~0.2 to ~4 keV, because the uncertainties in the calibration of the IPC beyond either end is considerably larger (Harnden et al. 1984). We also exclude the PH channel 1, regardless of its energy, because the calibration of PH channel 1 is far more uncertain than that of the other PH channels. The exact energy range depends on

the IPC gain during each observation (the energy boundaries of the PH channels vary as a function of the instrumental gain). We fitted our data to three models; thermal emission with Raymond emissivity and solar abundances, Bremsstrahlung emission, and power law. All models use the Brown & Gould absorption cross sections (1970). Throughout this paper, a power-law slope, α, means a photon index which is larger by 1 than an energy index.

The counts for the spectral fit were extracted from circles centered on the X-ray source centroid after excluding nearby sources. The radius was determined by inspecting radial profiles and X-ray images (see Paper I). The field background was estimated from surrounding annuli. This method of background subtraction is different from the one in Paper I, where we make use of background templates (which are provided by the *Einstein* Rev 1B Processing, Harnden et al. 1984). While suitable for subtracting the field background from the images for spatial studies and band flux derivation, using templates is not suitable for spectral studies. The reasons are that there may be spectral variations in the diffuse soft X-ray background from field to field (e.g., Trinchieri et al. 1986) and that these background templates made by the *Einstein* processing do not retain spectral information. Figure 1 shows that from the point of view of total background subtraction the local background method used here is equivalent to the method used in Paper I for most sources. To compare the two methods we have used the same energy band (0.2–3.5 keV) in both cases, by using the pulse invariant (PI) IPC bins. These are spectral bins with invariant energy boundaries. The counts detected in PH bins are mapped into PI bins as a function of the IPC gain (Harnden et al. 1984). This comparison shows that using the local background on-average does not produce systematic errors for our sample. However, for extended sources ($\gtrsim 10'$) in the center of the field of view the background derived from the surrounding circle could underestimate the real field background at the source position, because the effective mirror area decreases with the distance from the detector center due to the telescope vignetting and therefore the diffuse sky component of the background is reduced. To correct this problem, we used a mean IPC field background template and calculated the ratio of total counts within the source circle and background annulus. We rescaled the background counts by multiplying by this ratio the background PH counts, which were then subtracted from the source counts. Strictly speaking, the correction should be computed for each field because it depends on the relative amounts of diffuse and particle background. However, this is a second order effect, and given our results (see below) not worth pursuing. We applied this procedure in the most significant four cases, NGC 1399, 5044, 5548, and 7619. However, because the extended sources are also strong sources, this correction does not change significantly the derived spectral parameters. For NGC 5044 the parameter ranges are identical, while for the other three cases the corrected data give similar kT (or α), but the $N_{\rm H}$ ranges extend towards higher values.

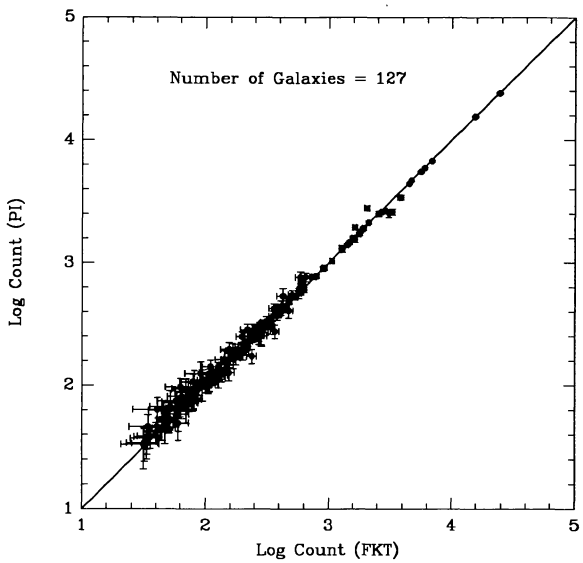

FIG. 1.—Comparison of net counts estimated with local background subtractions (PI) and net counts derived by using the background map (FKT; Paper I) for all the galaxies analyzed in this paper.

We applied the two-parameter model fitting to all the galaxies listed in Paper I detected with more than 50 net counts. In many galaxies, however, the error of an individual parameter is large and in the worst case the whole range of kT and $N_{\rm H}$ is acceptable within the error. We find that the spectral parameters are reasonably constrained only in galaxies with $\gtrsim 300$ counts. We, therefore, present the results only for galaxies with more than 300 net counts. Additionally, NGC 4552 (with 280 net counts) is included because its spectral parameters are relatively well determined. To fit the data we used the DGNI gain map, which is appropriate for extended sources.

In Figures 2, 3, and 4, we show the significance contours for each model fit for ellipticals, spirals and AGN. We put S0 galaxies with ellipticals throughout this paper (comparisons between finer morphological types are described in Paper III). We show our results for a total of 43 galaxies (45 observation sequences). Also shown is the observed distribution of spectral counts in the IPC with the best-fit spectrum. We show a comparison with an optically thin Raymond spectrum for elliptical galaxies, which tend to have low emission temperature (see § 2.2). We use a bremsstrahlung model for spirals; this model has been used for spectral fits of spirals in the literature (for example, see Fabbiano & Trinchieri 1987). Similarly, we show a comparison with a power-law model for AGN.

The results of the IPC spectral fits are summarized in Tables 1, 2, and 3, for E and S0 ($T = -5$–-1), spirals ($T = 0$–10), and AGN, respectively. These tables have the same format. In each we list: galaxy name; morphological type (T from Sandage & Tammann 1981 or de Vaucouleurs, de Vaucouleurs, & Corwin 1976); R.A. and Decl. (1950); observation sequence; exposure times; source and background regions; off-axis distance in arcmin; net counts with statistical errors; IPC gain; PH channels and corresponding energy ranges used in the fit; ranges of spectral parameters (kT or α, and $N_{\rm H}$) at the 90% confidence level; Galactic $N_{\rm H}$ (Stark et al. 1992); minimum χ^2; and number of degrees of freedom. For two galaxies (NGC 4151 and NGC 6946) observed more than once, each observation is presented separately. We list 21 ellipticals in Table 1 and 16 spirals in Table 2. Our sample included 17 additional galaxies with active galactic nuclei (AGN; strong nuclear X-ray point sources and optical emission line spectra). Most of these galaxies are included in the paper by KUC and our results are

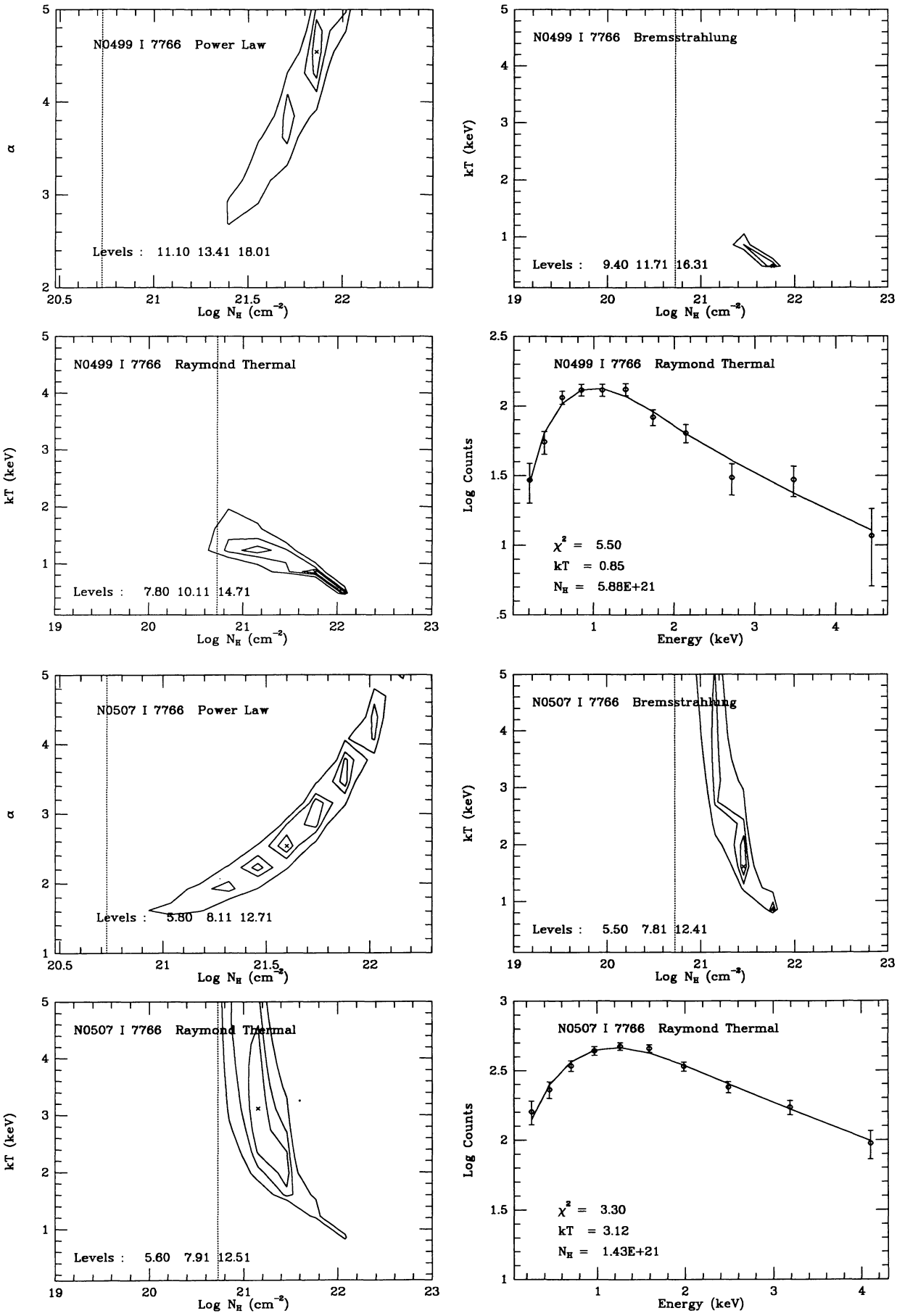

FIG. 2.—χ^2 contours with kT and N_H grids for elliptical galaxies. Three models (*upper left:* power law; *upper right:* Bremsstrahlung; *lower left:* Raymond thermal) are used to fit the data. The best-fit spectrum calculated with Raymond thermal model is compared with the observed data in lower right panels. The three contours (*inner to outer*) represent the 68%, 90%, and 99% confidence levels for two significant parameters (Avni 1976) and the cross mark is at the best-fit parameters. The vertical dotted line indicates the galactic H I column density (Stark et al. 1992).

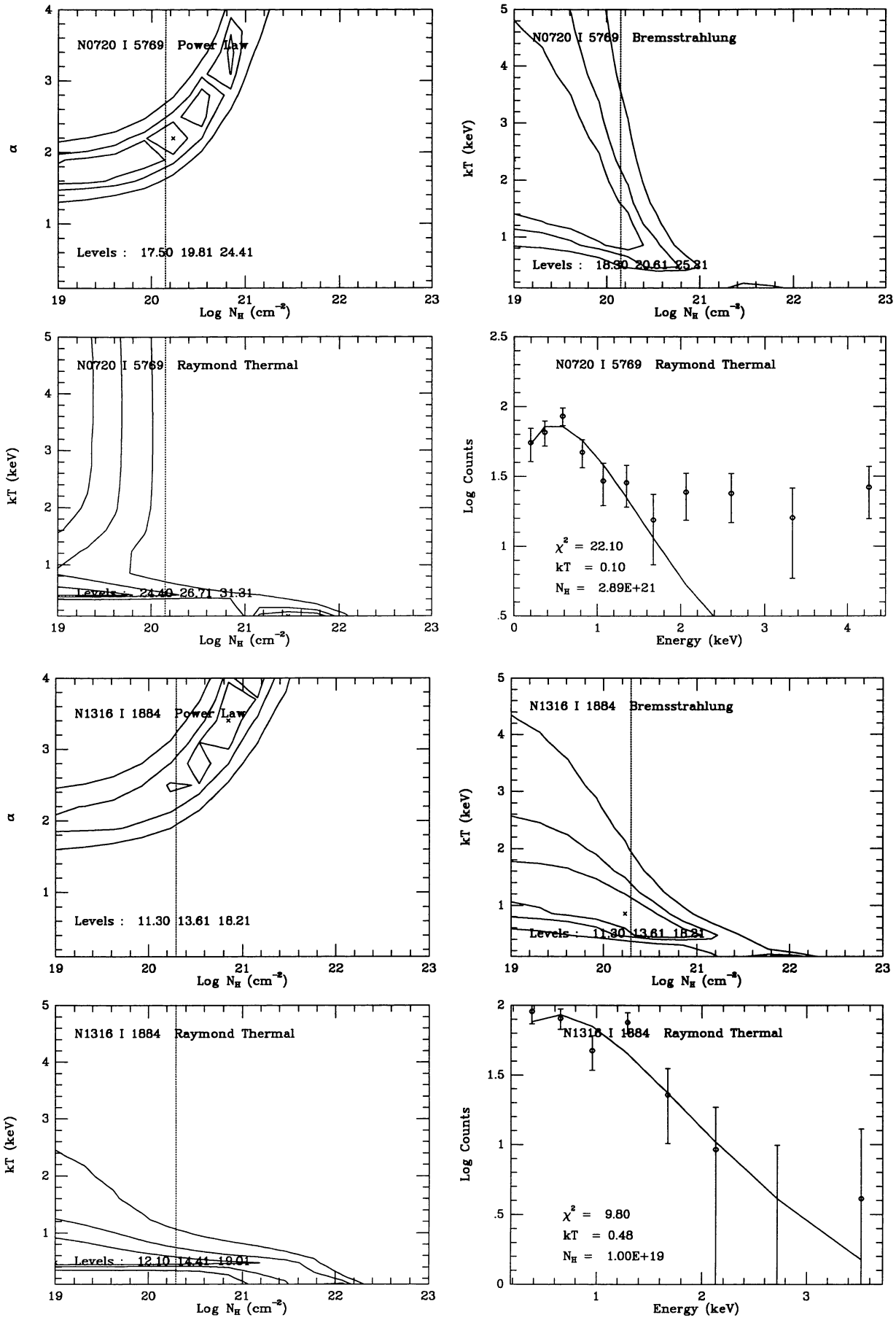

FIG. 2—*Continued*

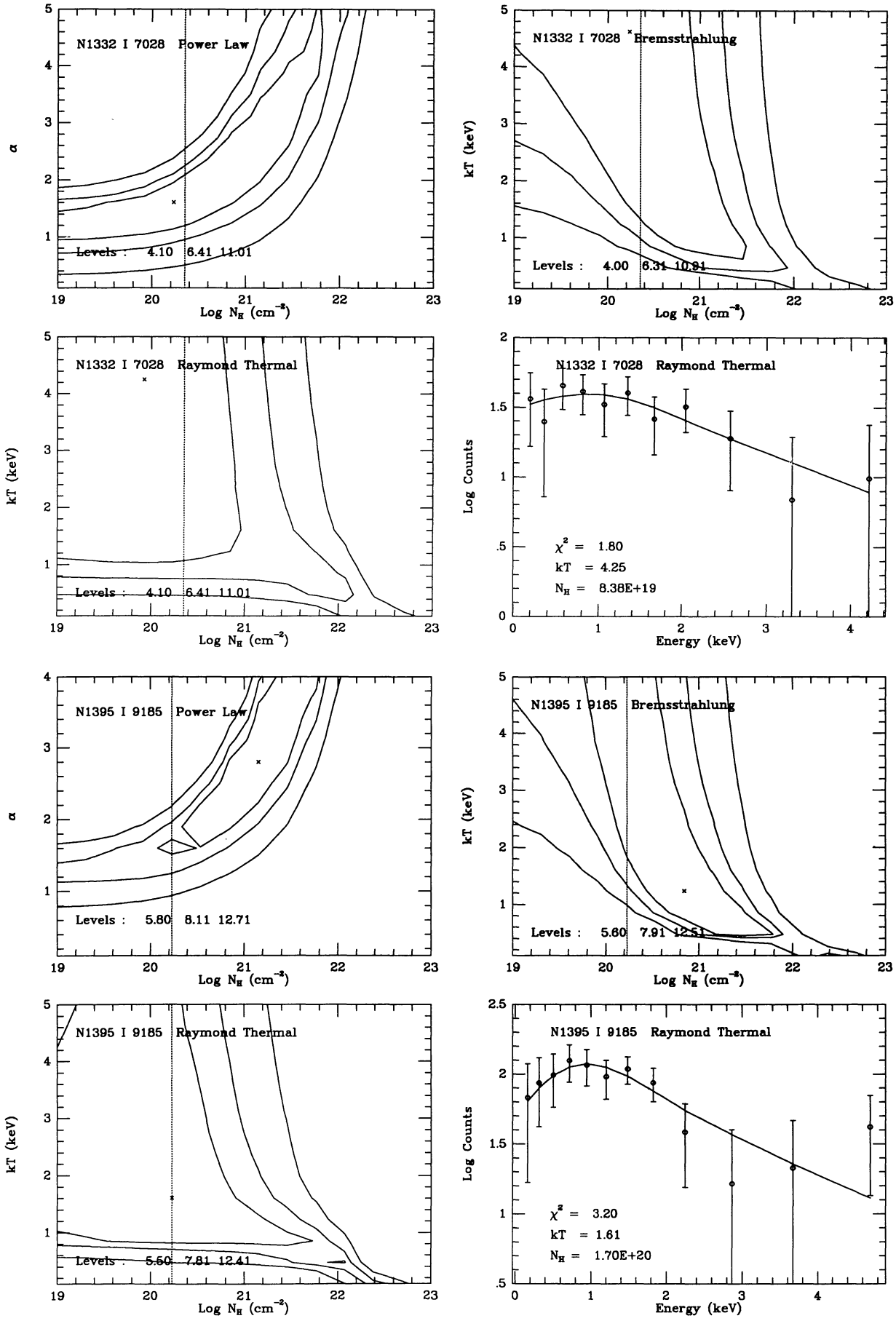

FIG. 2—*Continued*

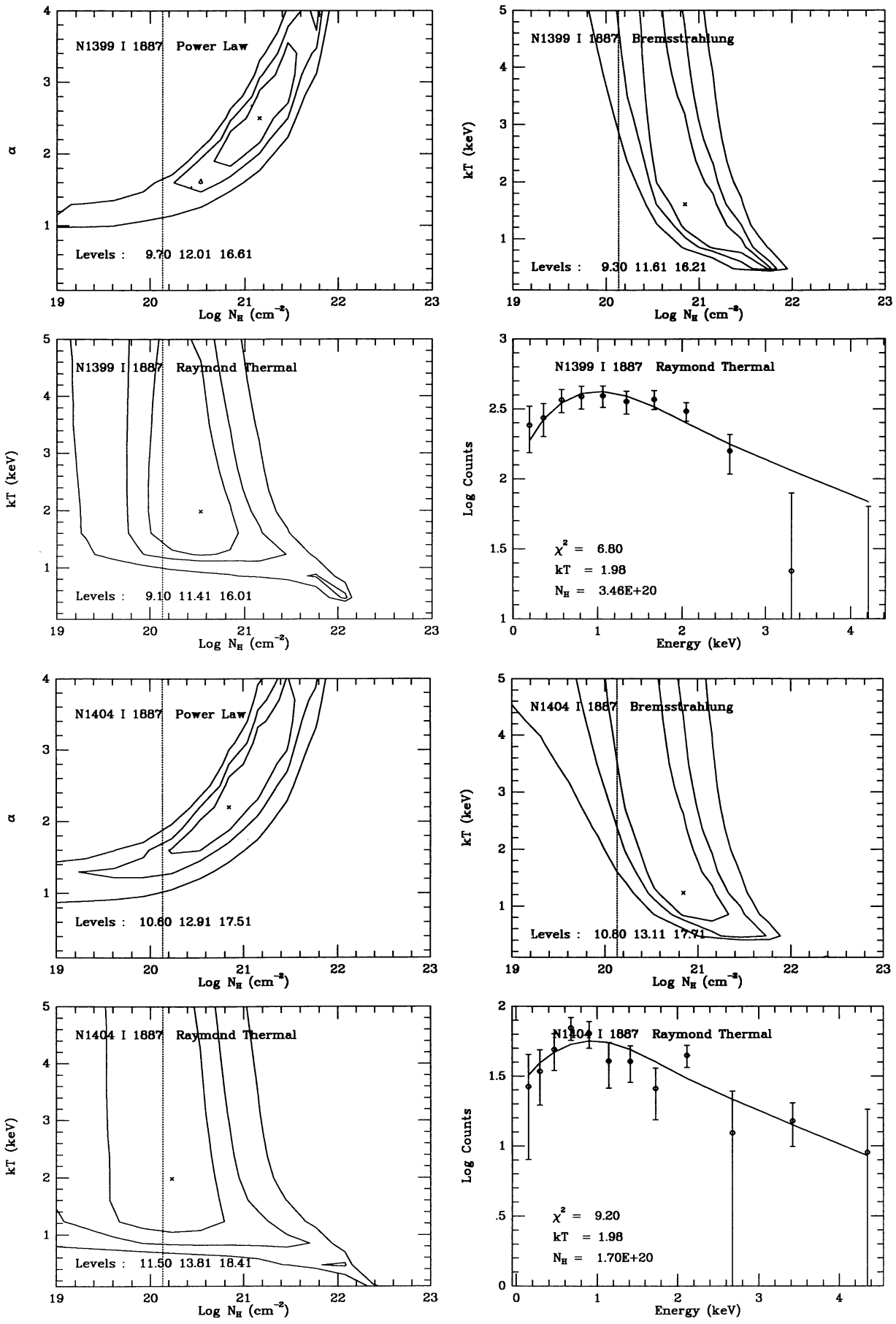

FIG. 2—*Continued*

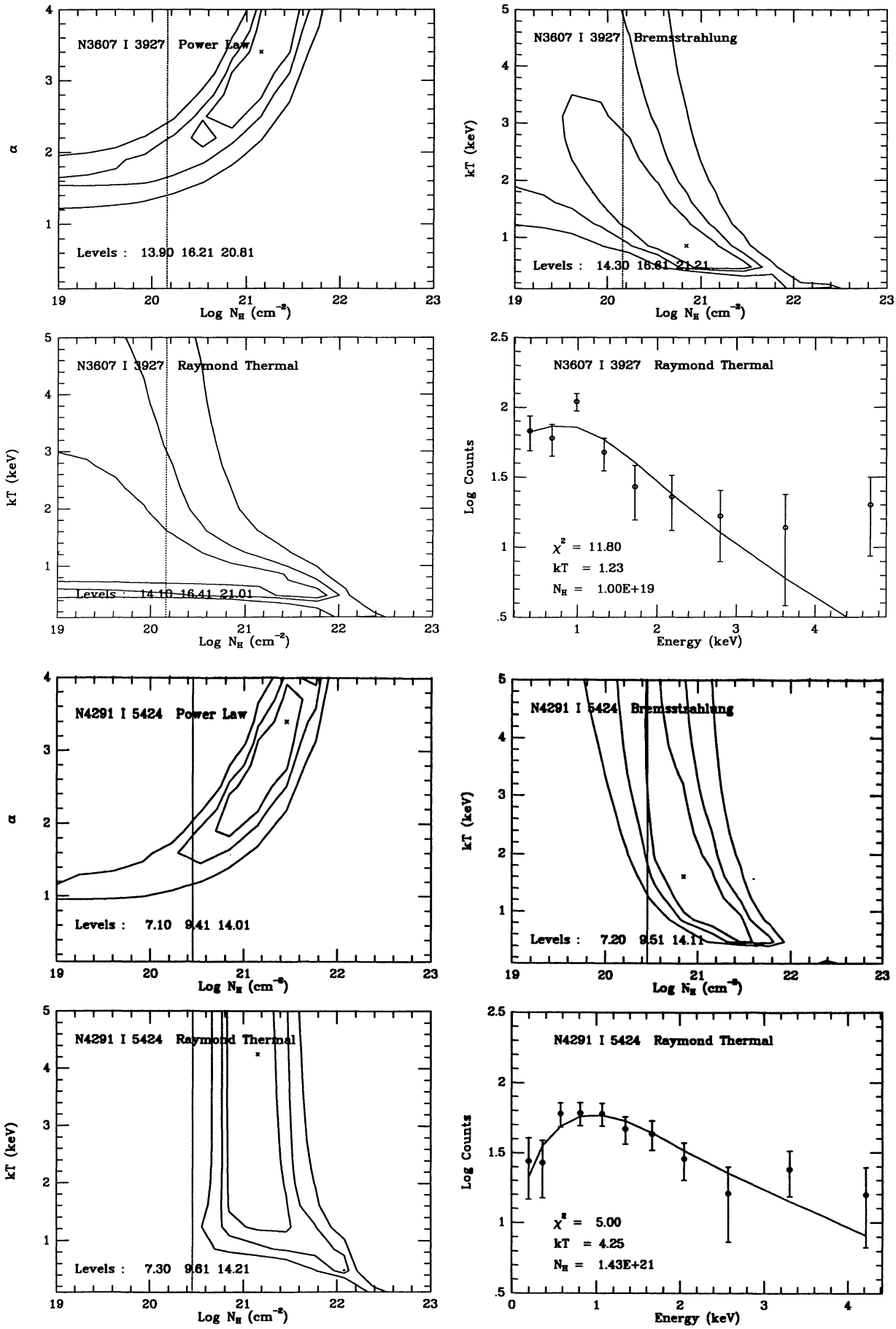

FIG. 2—*Continued*

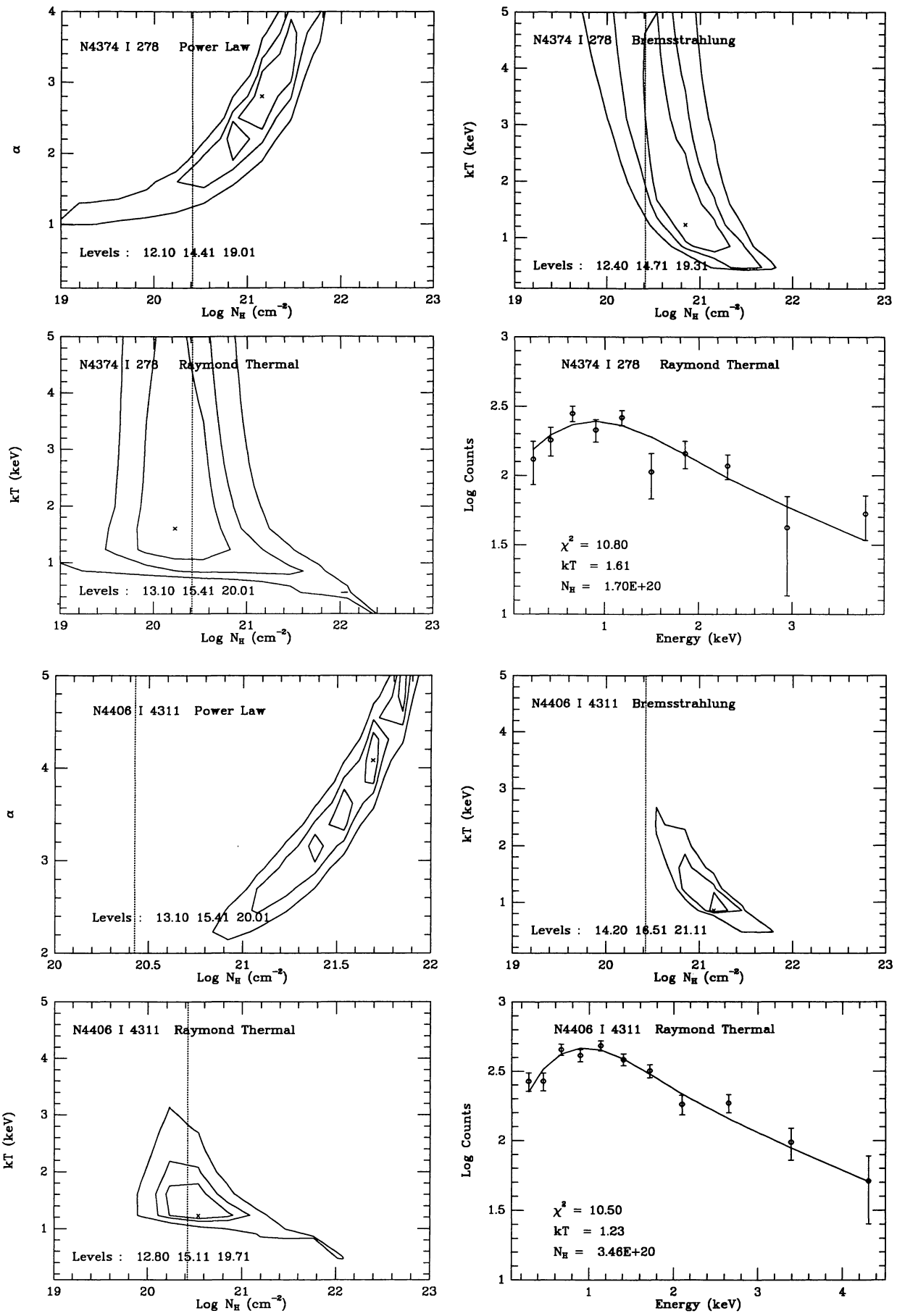

FIG. 2—*Continued*

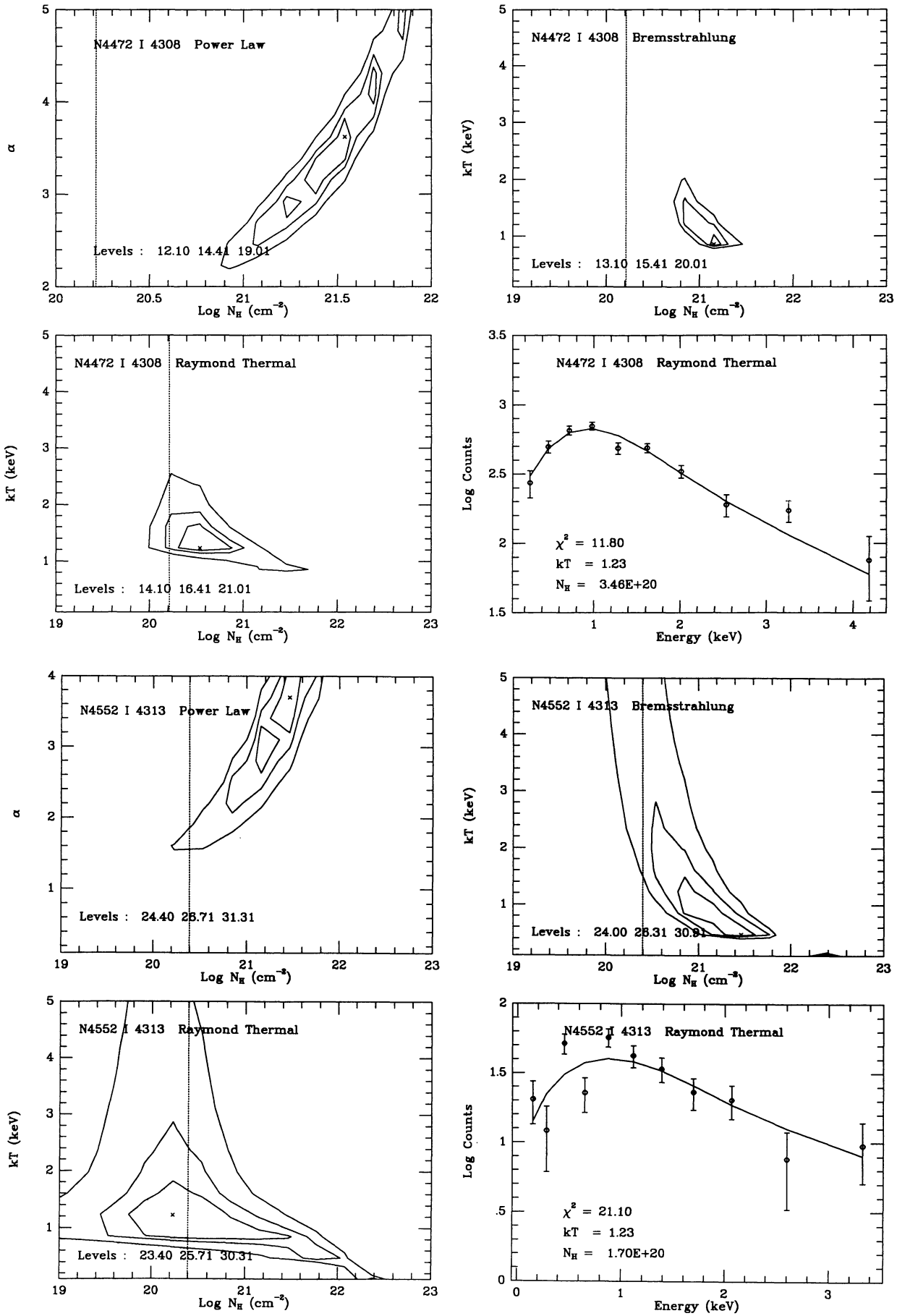

FIG. 2—*Continued*

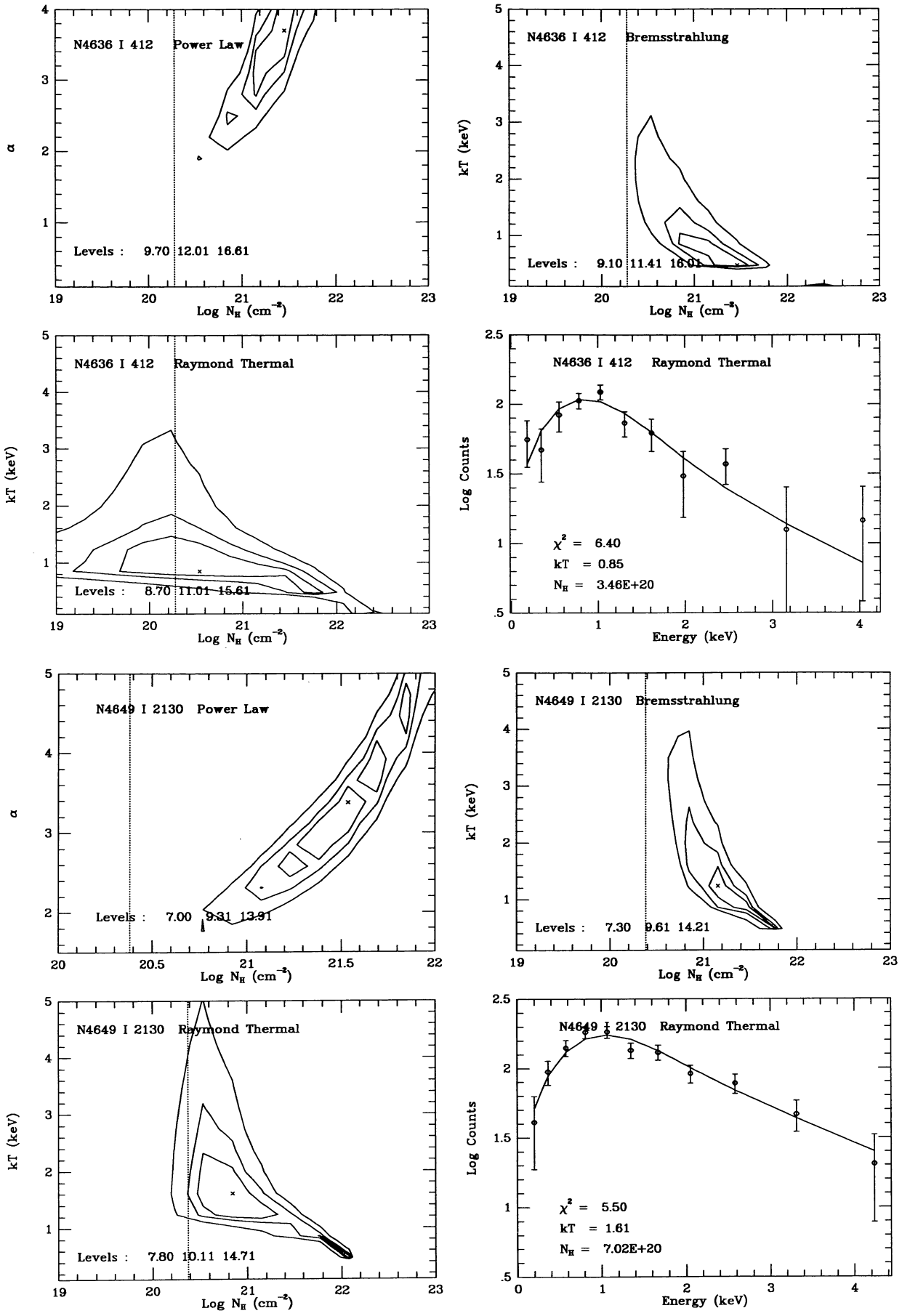

FIG. 2—*Continued*

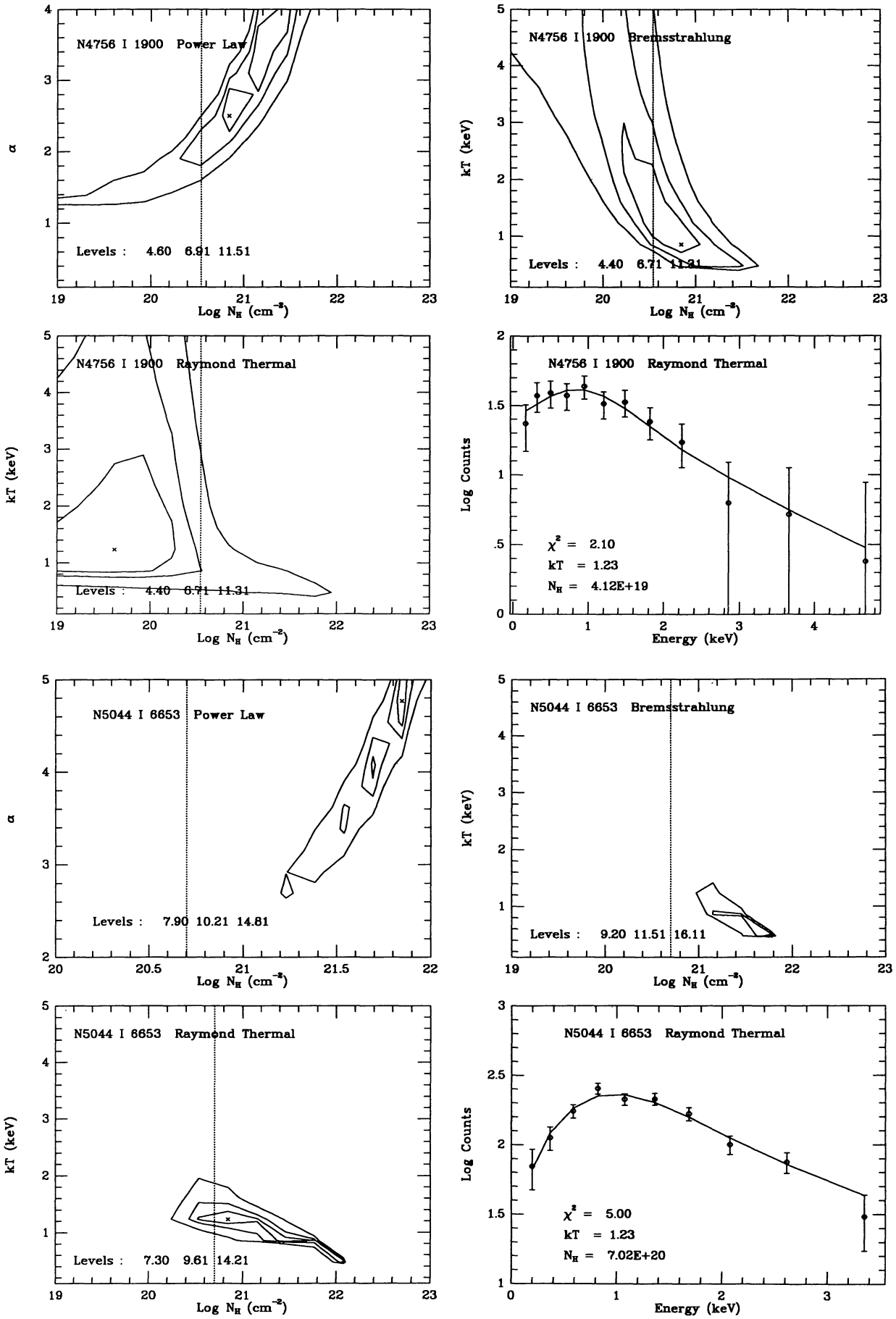

FIG. 2—*Continued*

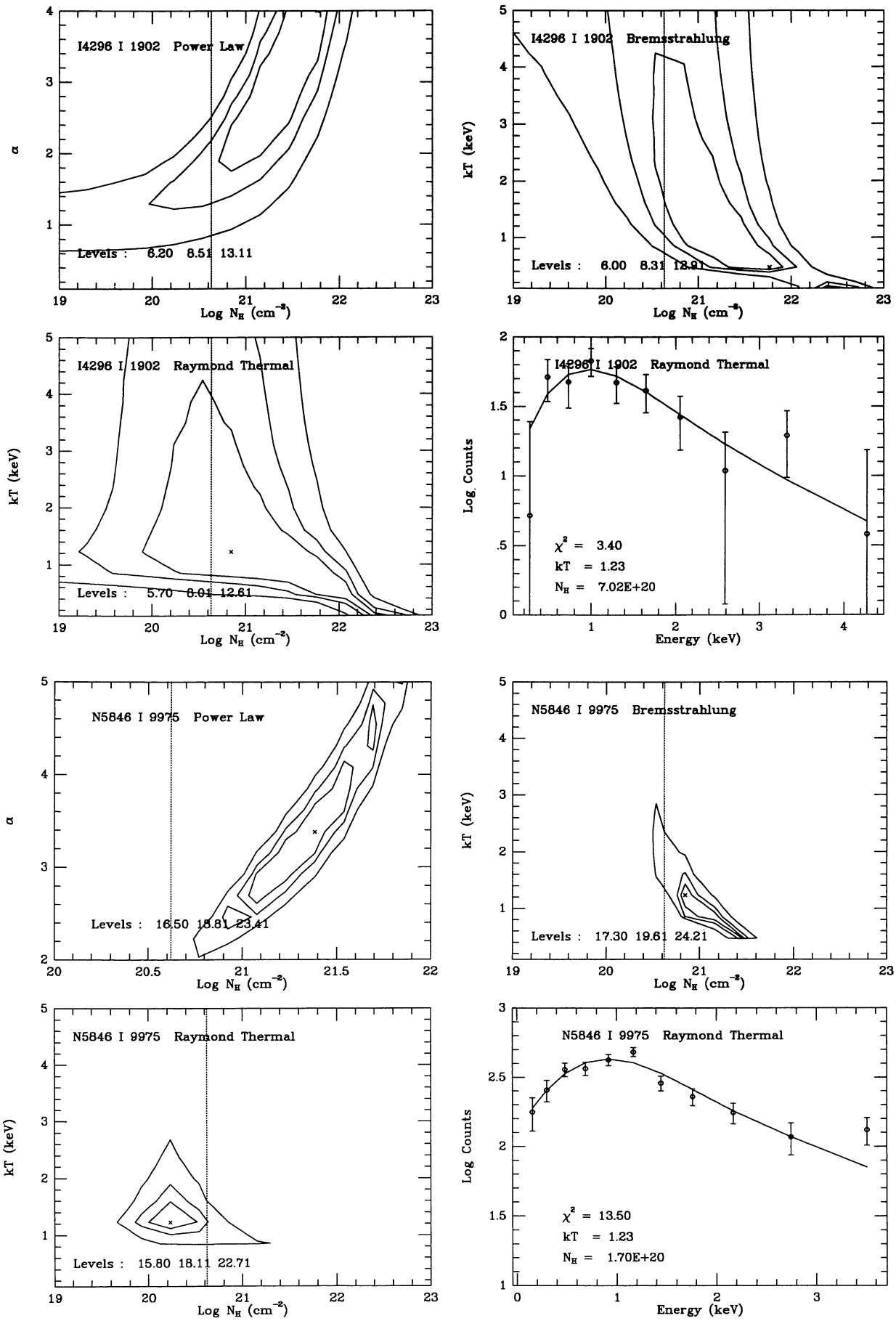

FIG. 2—*Continued*

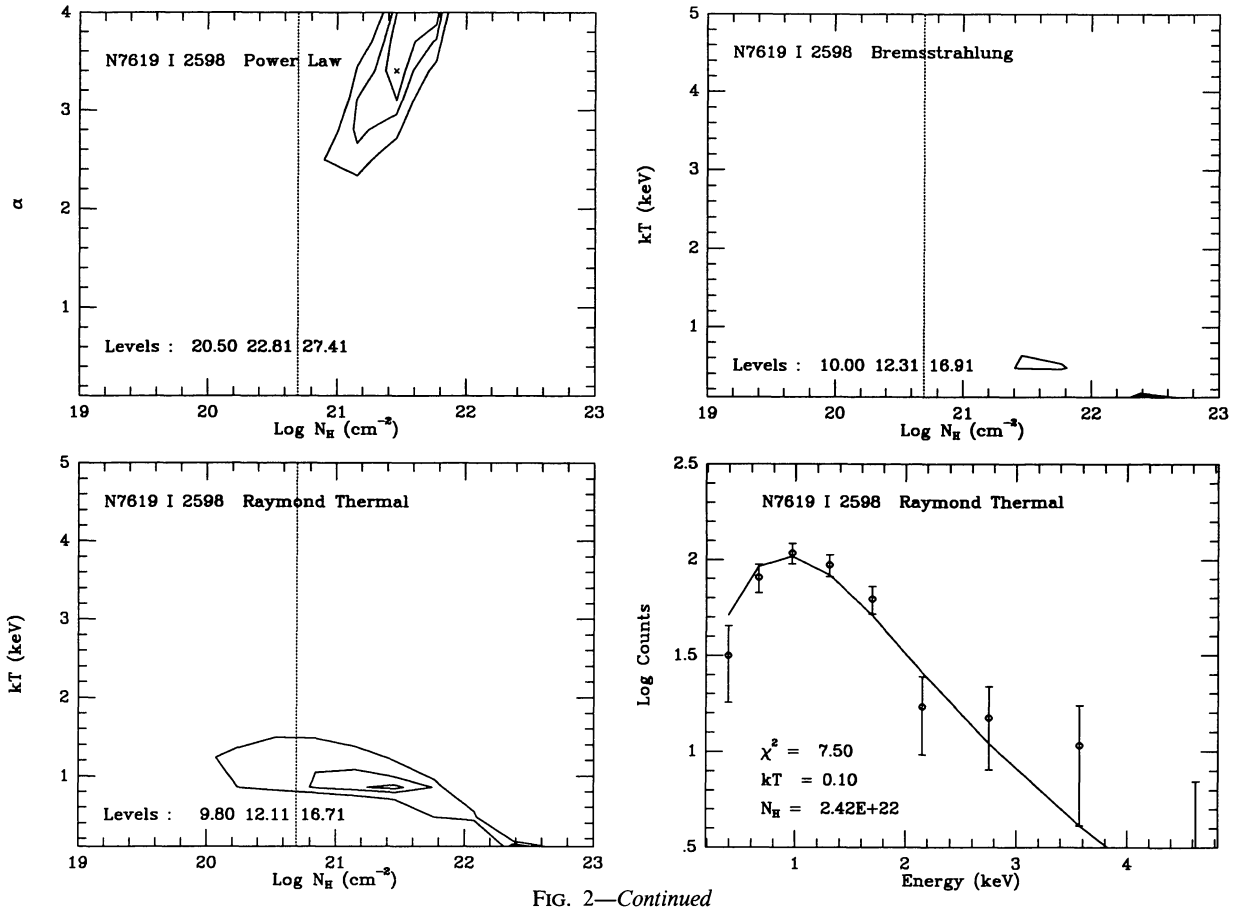

FIG. 2—*Continued*

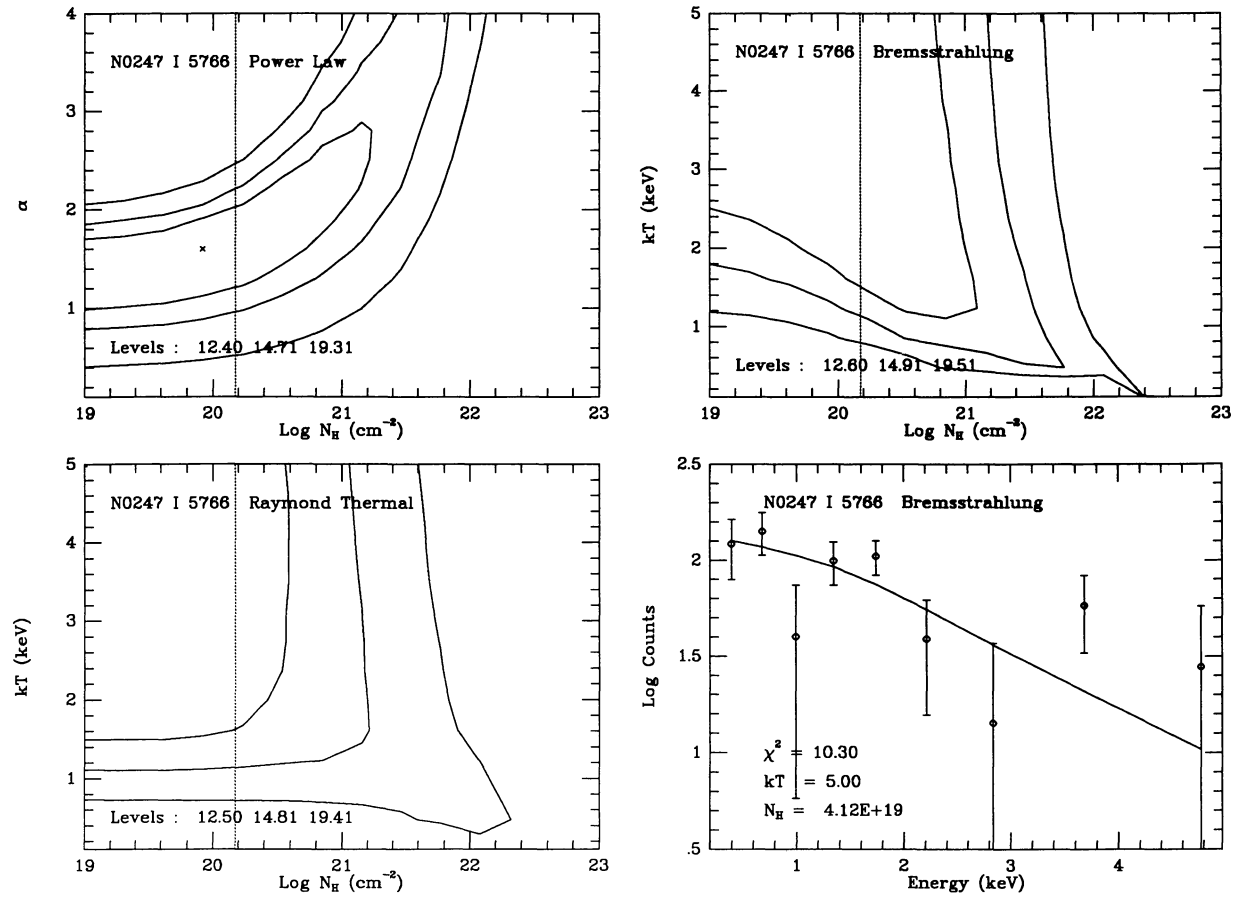

FIG. 3.—Same as Fig. 2, but for spiral galaxies. In lower right panels, a bremsstrahlung model is used.

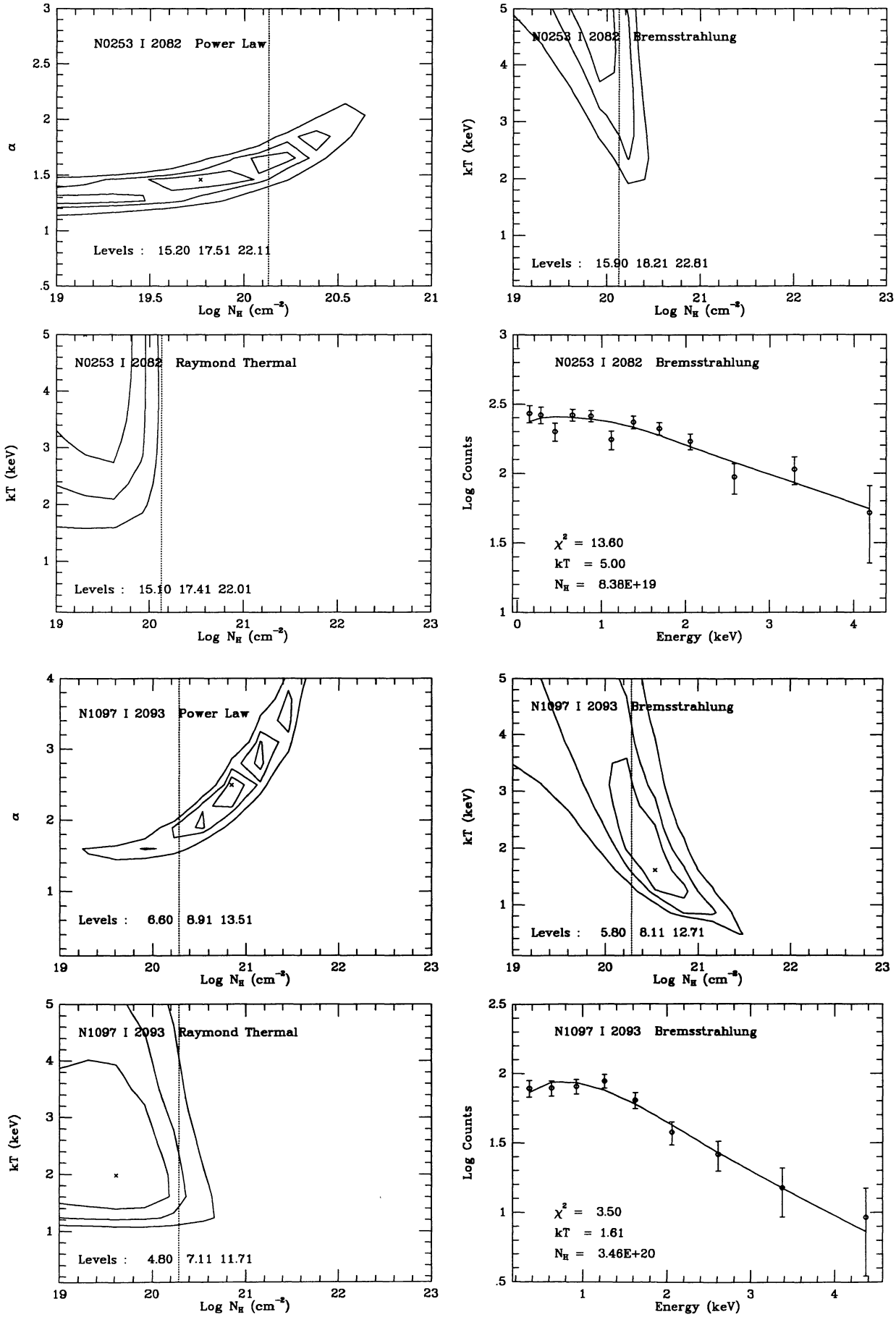

FIG. 3—*Continued*

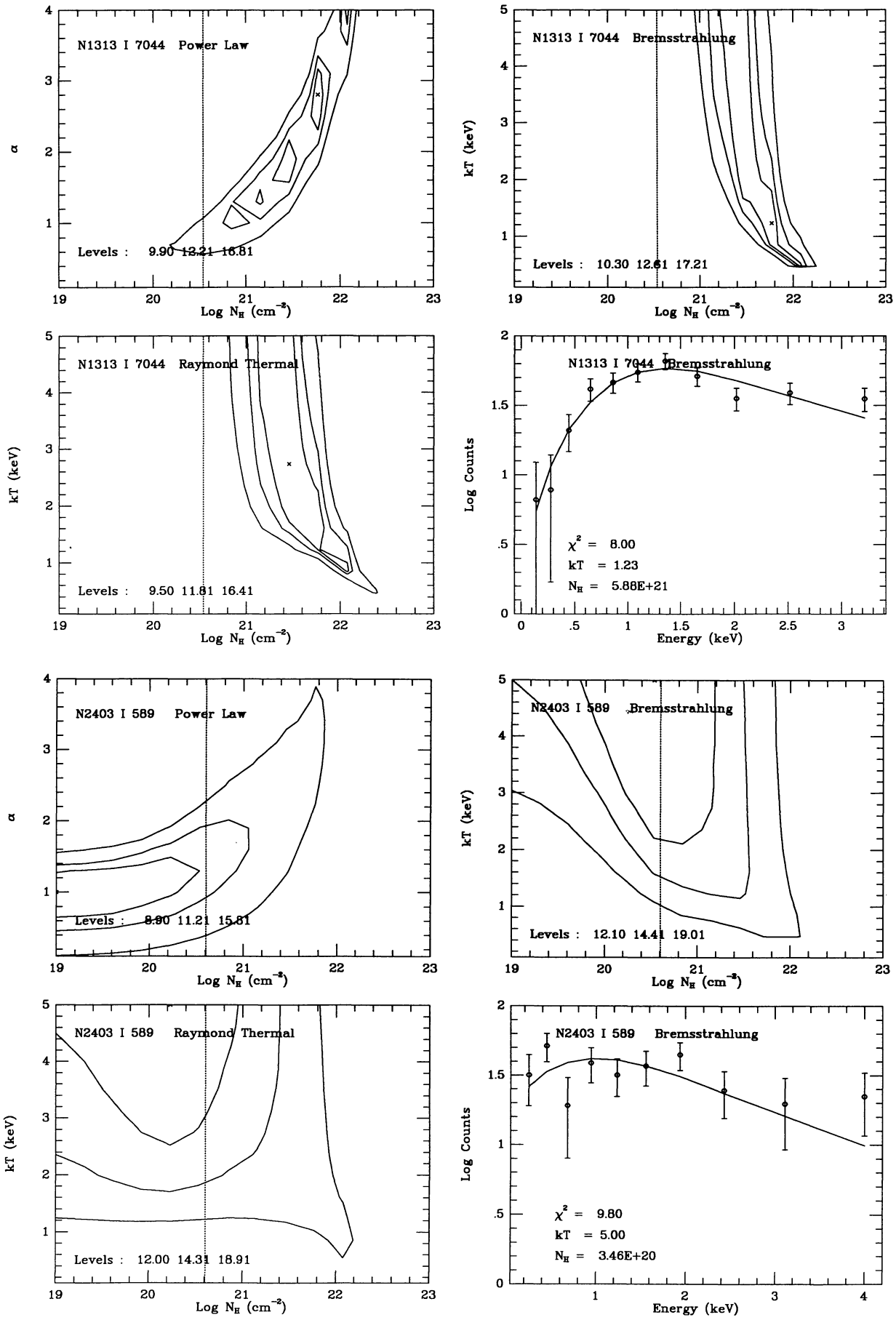

FIG. 3—*Continued*

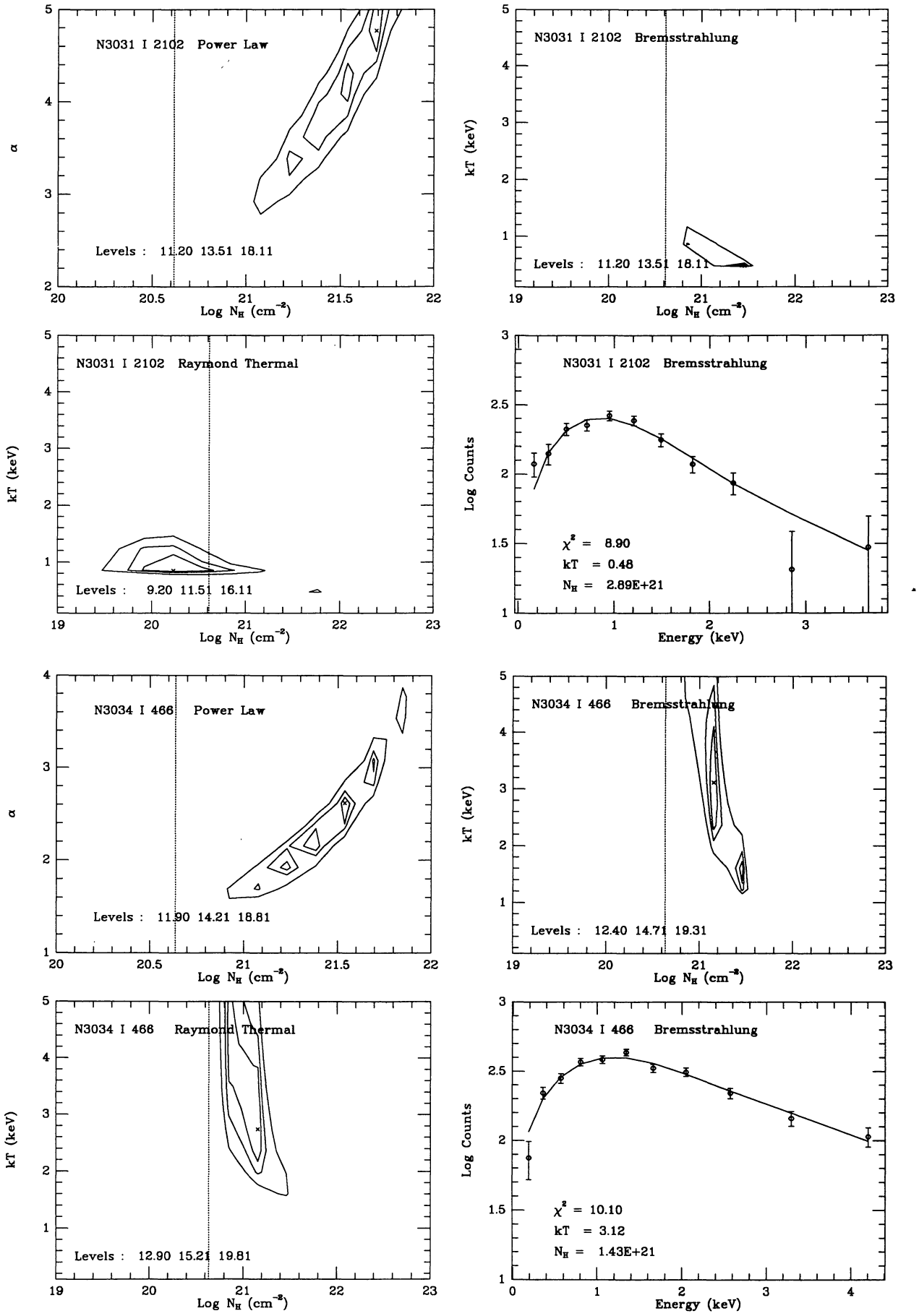

FIG. 3—*Continued*

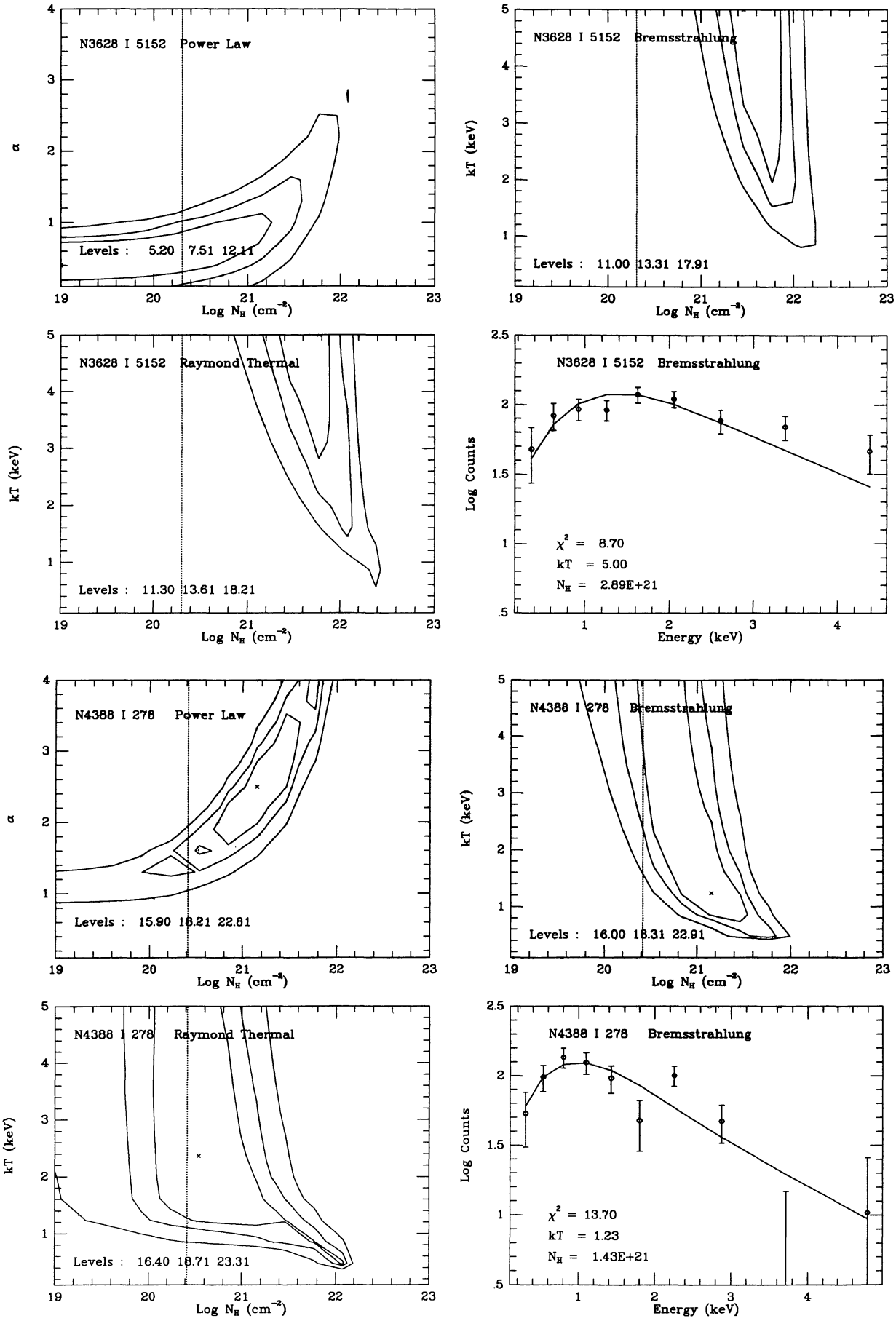

FIG. 3—*Continued*

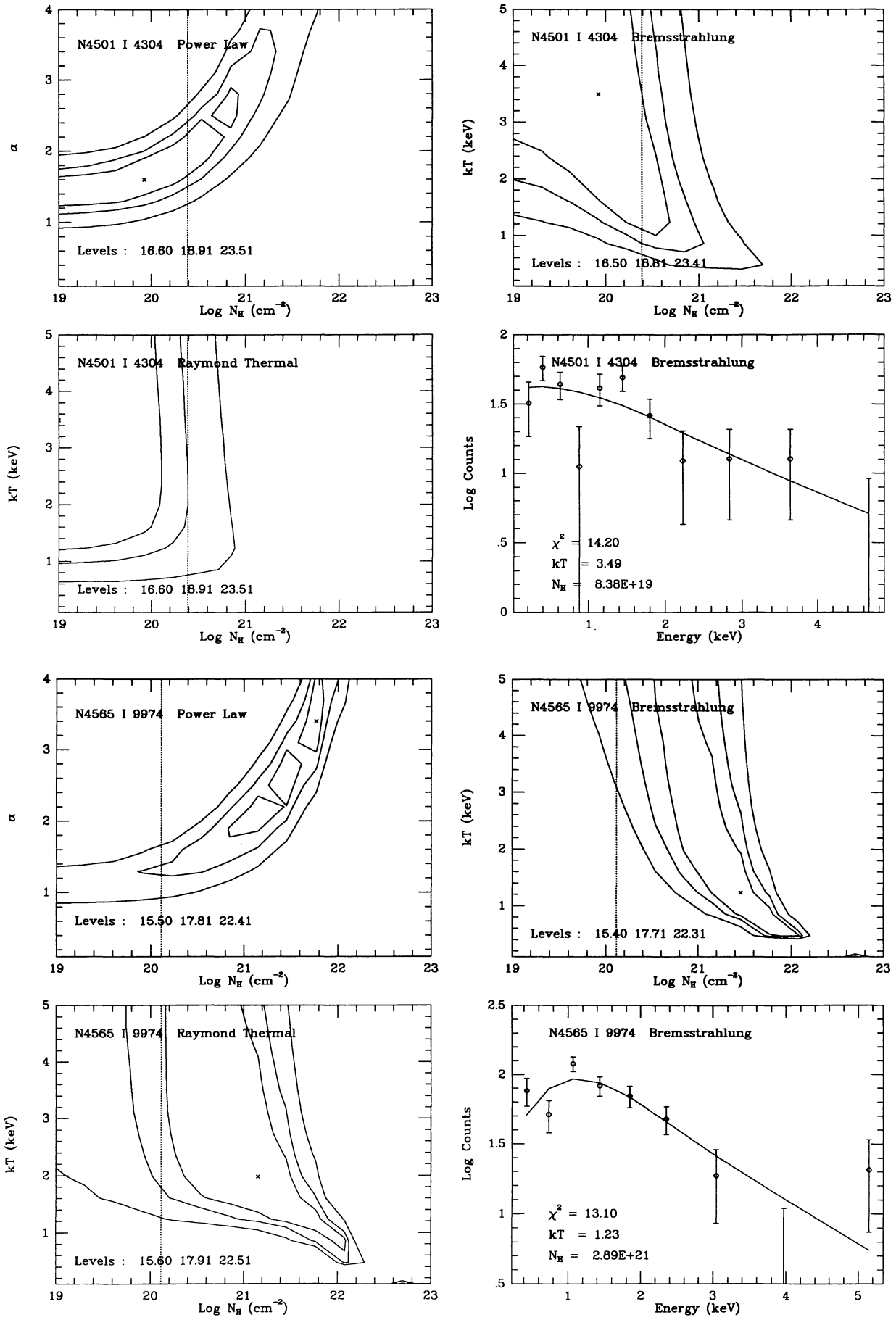

FIG. 3—*Continued*

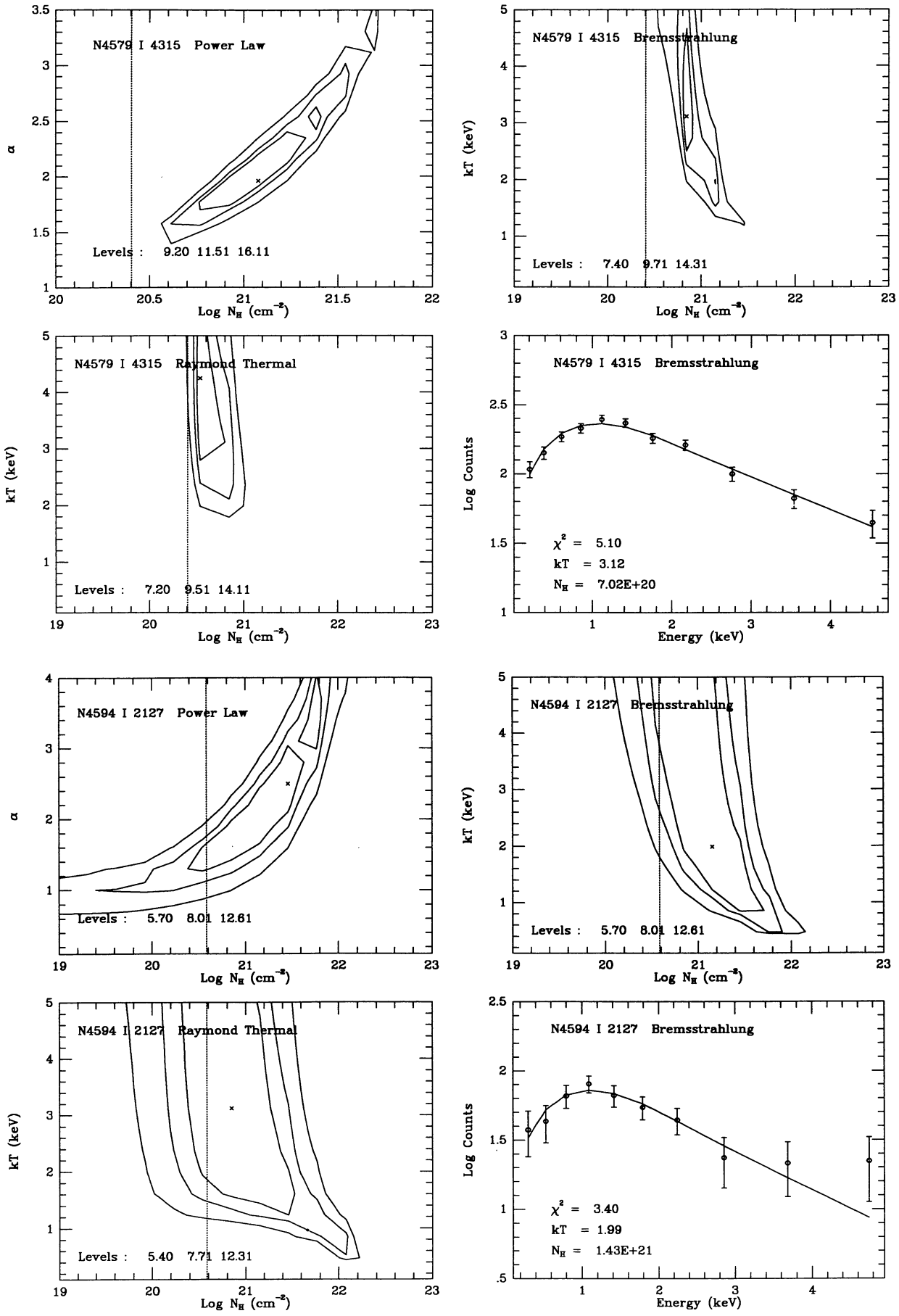

FIG. 3—*Continued*

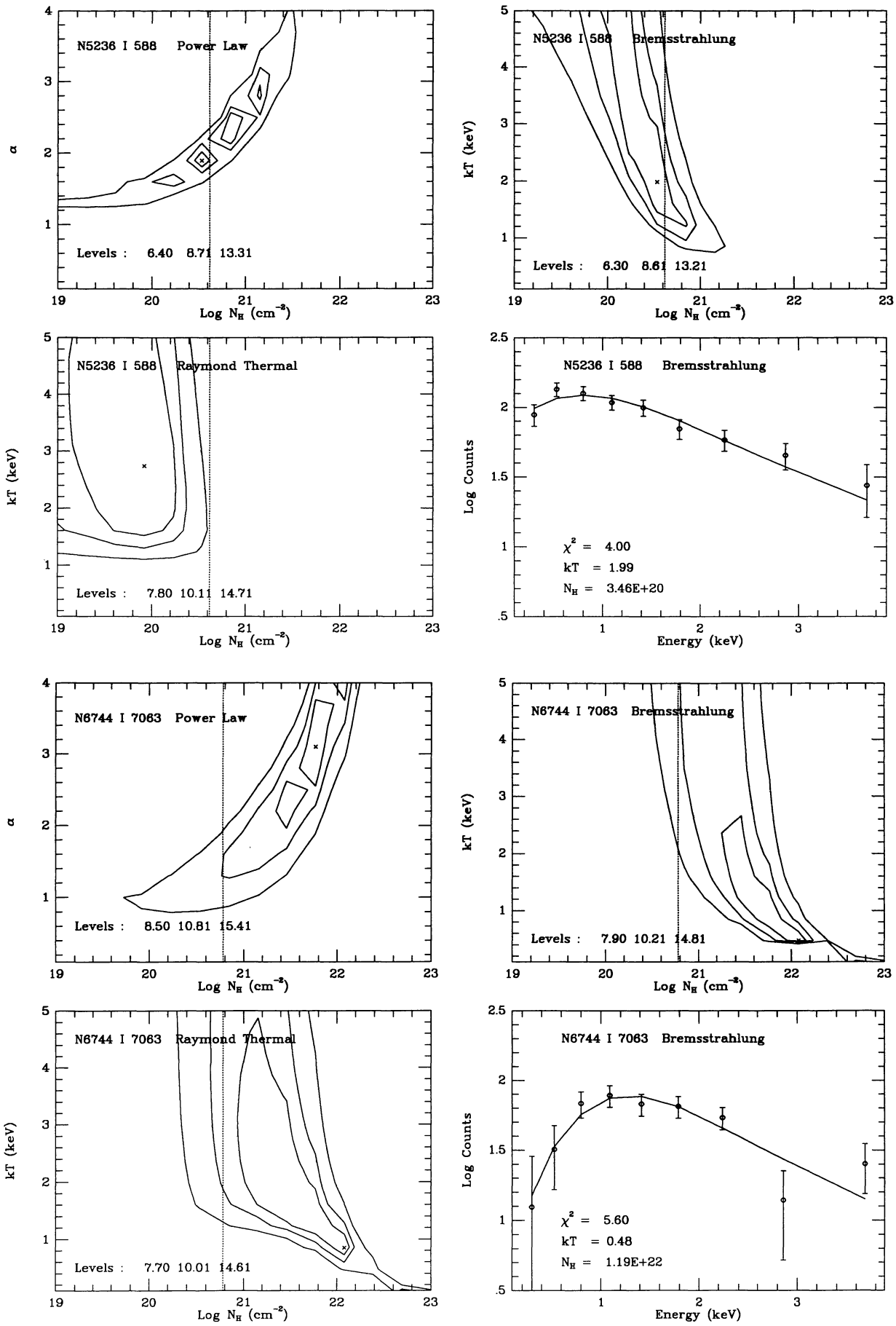

FIG. 3—*Continued*

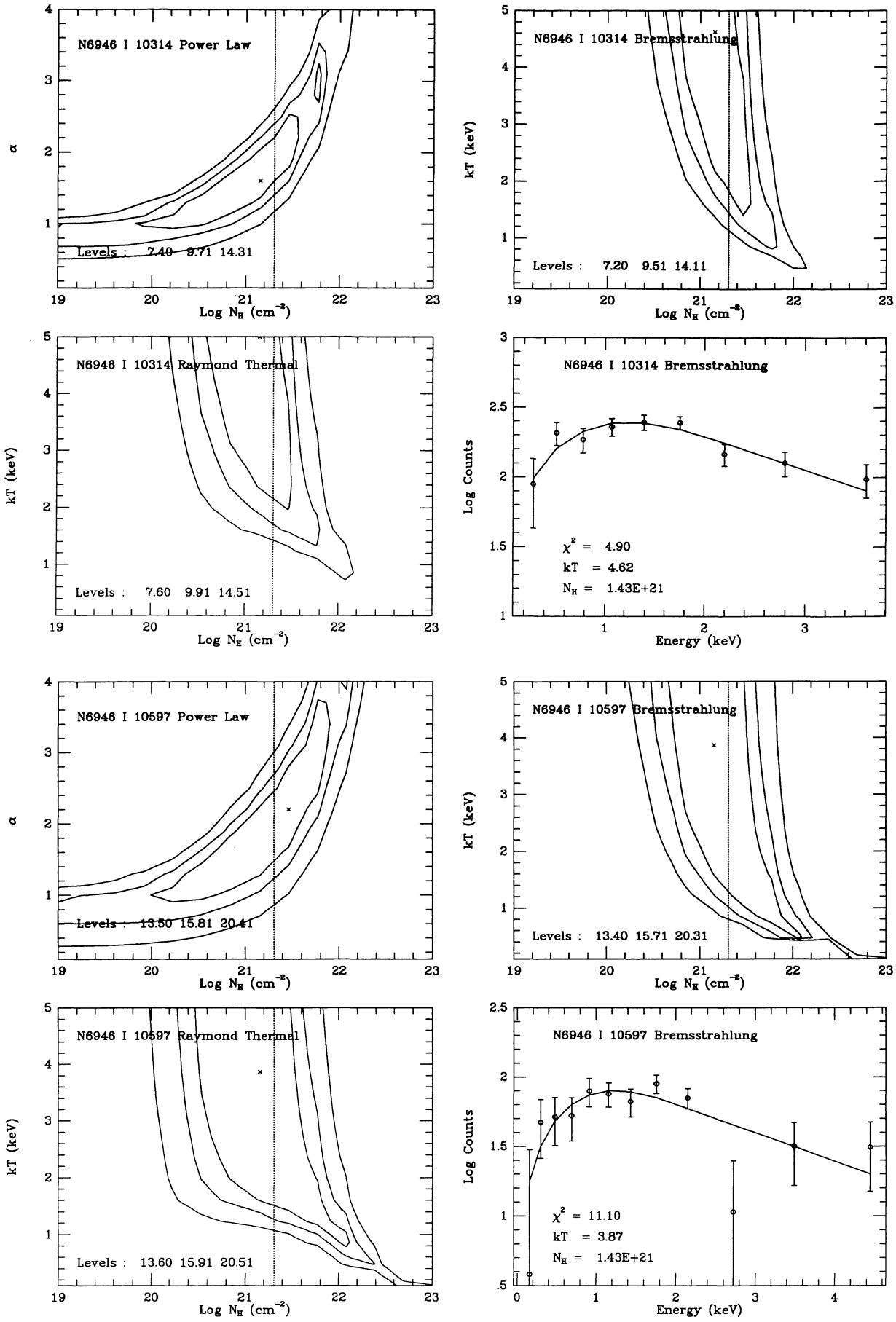

FIG. 3—*Continued*

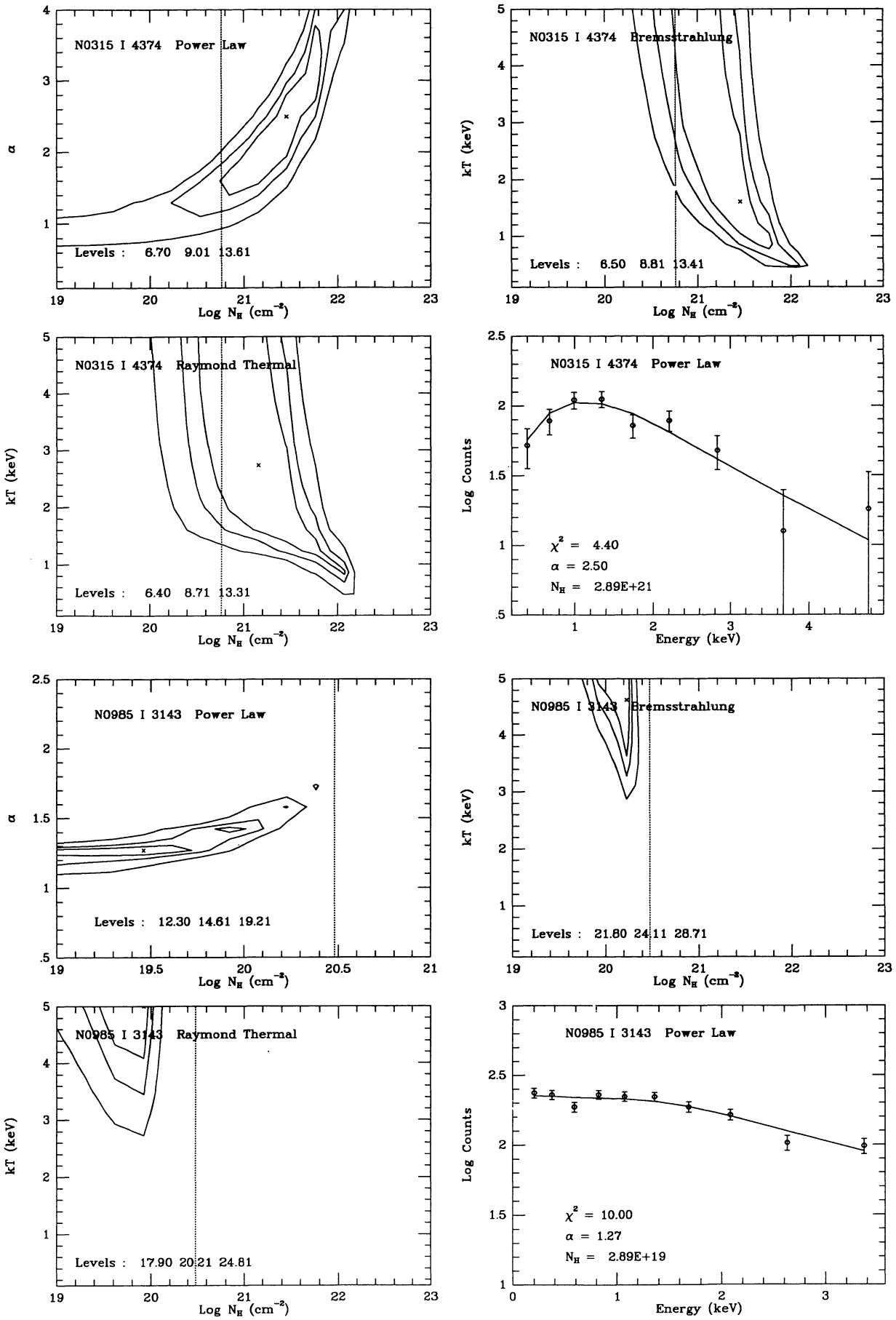

FIG. 4.—Same as Fig. 2, but for AGNs. The y-axis is a power-law photon index α. In lower right panels, a power-law model is used.

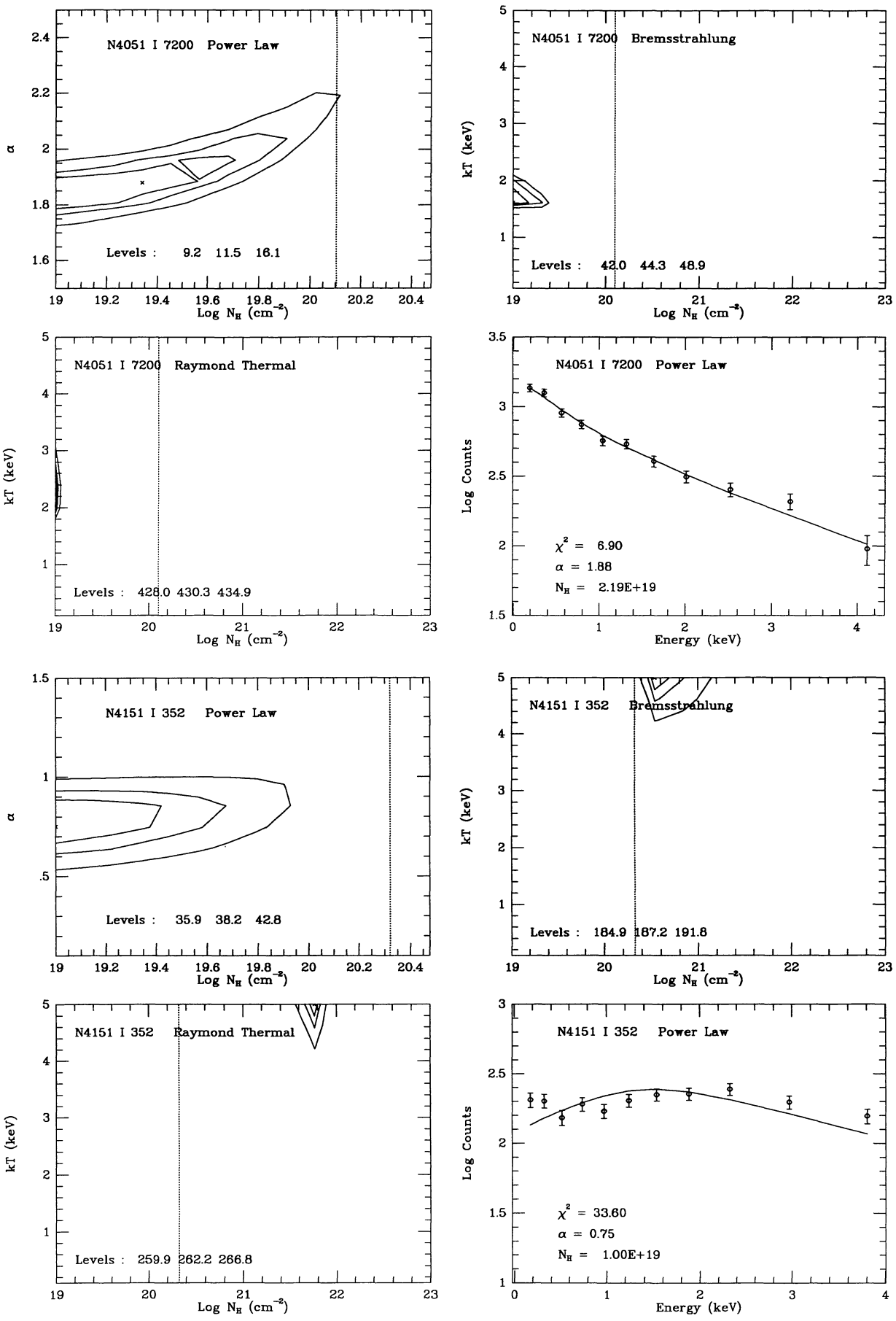

FIG. 4—*Continued*

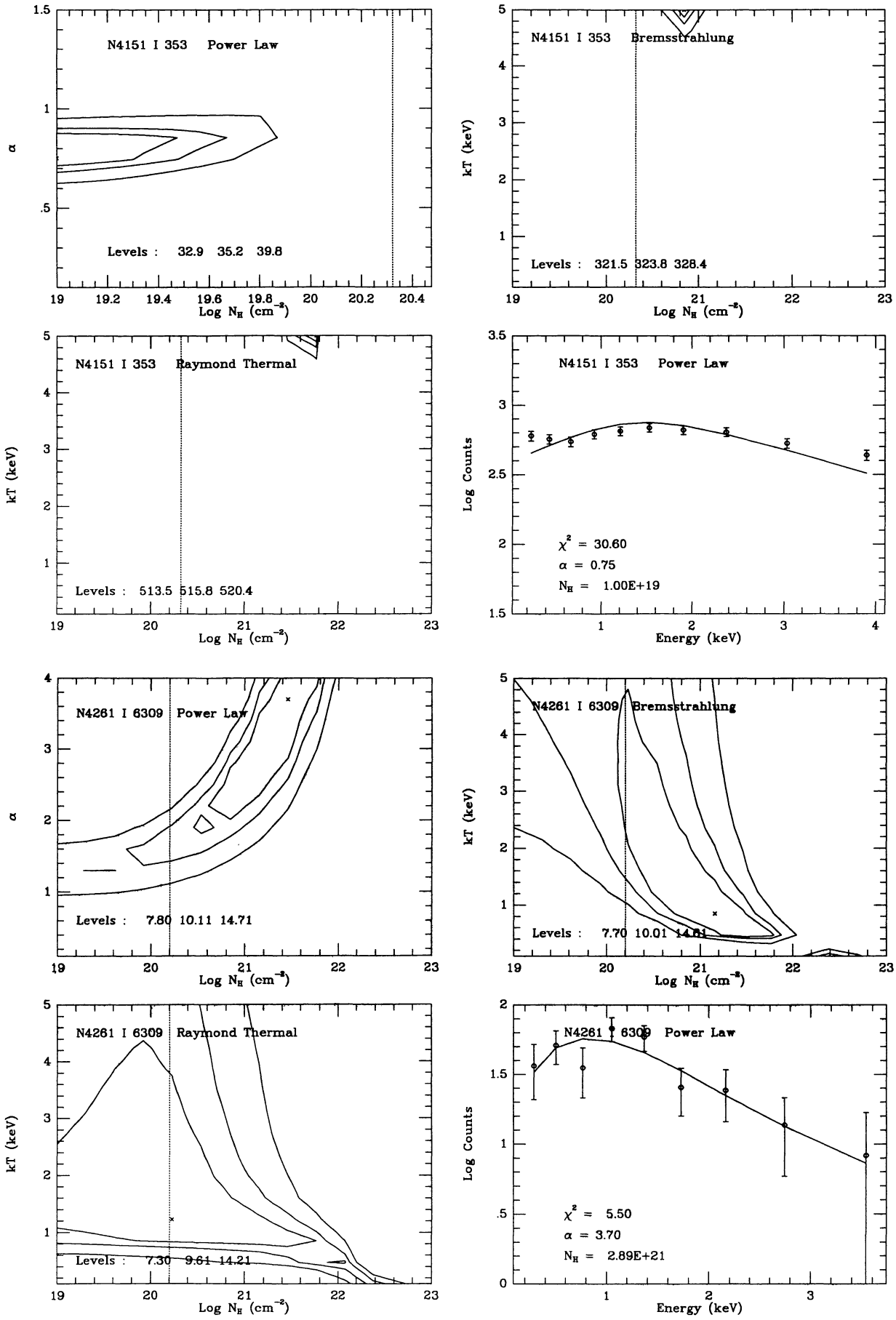

FIG. 4—*Continued*

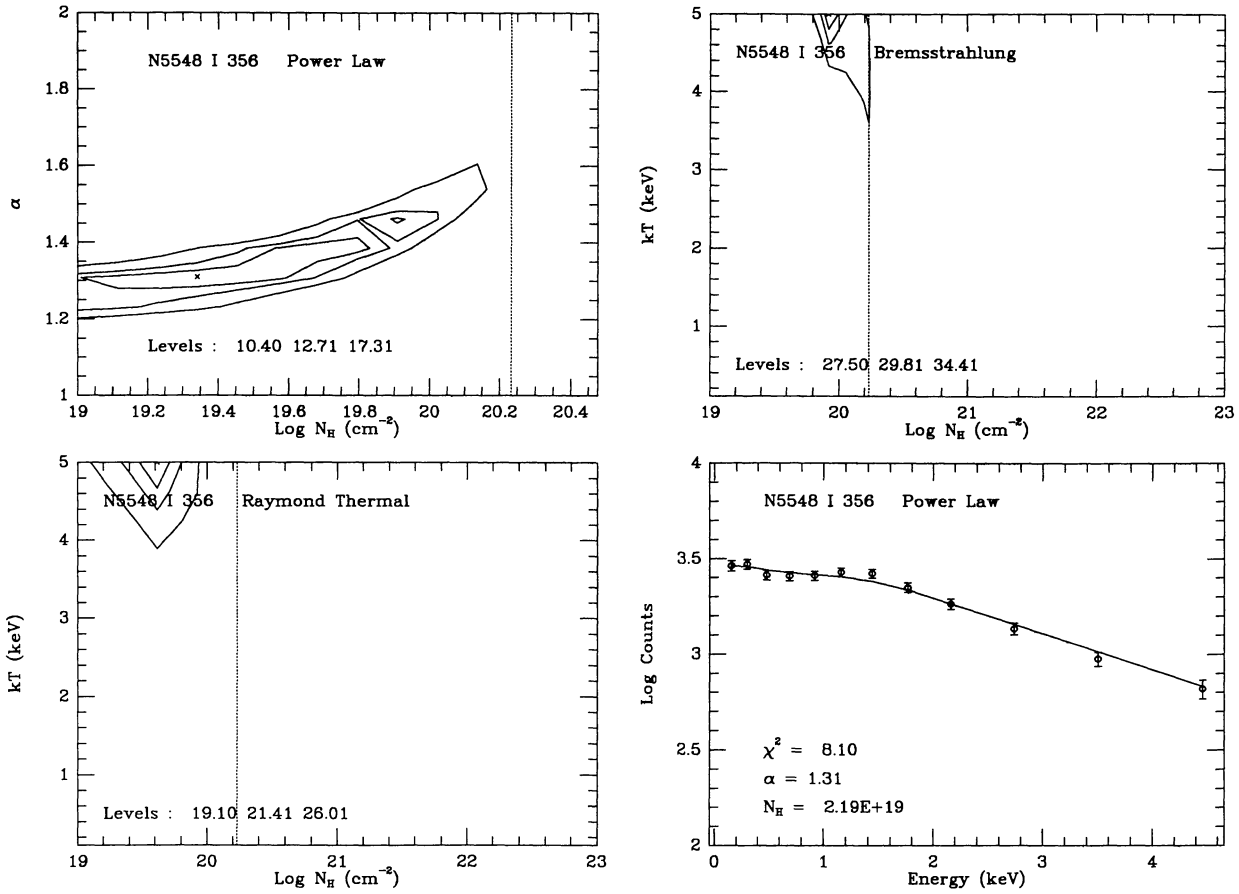

FIG. 4—*Continued*

consistent with theirs. We, therefore, do not present them in this paper. We list instead in Table 3 six galaxies belonging to this sample which are not included in KUC or for which our analysis has given different results.

In Table 1, we present the results of the fit to a Raymond (optically thin continuum and lines) spectrum, which is appropriate for gaseous halos, such as may be present in at least some of the large elliptical galaxies. In Table 2 we give instead the results of the fit to a bremsstrahlung model (exponential plus gaunt factor). This type of spectrum has been used to describe the properties of binary X-ray sources which presumably dominate the emission in spirals. In Table 3, we list the results of the fit to a power law for galaxies whose emission is clearly dominated by a pointlike nuclear source. Power-law spectra are typically used to describe the nonthermal emission which predominates in these galaxies (for example, see KUC).

For several galaxies, the IPC gain varied significantly during the observation. The main reason is that a particular sequence might contain data taken at separate time intervals. If the gain changes more than 10% from the time averaged mean, the image was regenerated into two to three segments of a constant gain and the model fitting was applied to each segment. These observations are marked in Table 1 and gain changes are listed in the notes (§ 4). Usually the spectral fit with the whole observation is as good as that with the segment of the longest exposure. A 3% systematic error (F. R. Harnden 1991, private communication) was added in quadrature to the statistical error of strong sources (NGC 4051, 4151, and 5548). For these galaxies the statistical error is smaller than the systematic error, while for the other galaxies the systematic error is negligible compared to the statistical error.

There are a few unusual spectra (NGC 720, N4151, N4552) which do not fit to the model with high statistical significance. NGC 720 appears to have extra hard photons (see Fig. 2). These hard photons are mainly coming from large radii ($r \gtrsim 3'$), where several X-ray emitting blobs are present (see Paper I). The spectrum of the inner region ($r < 3'$) gives a better fit to the thermal model ($\chi^2 = 12.8$ and degree of freedom = 8) with $kT = 0.48$ keV (<0.8 keV at 90% confidence) and $N_H = 7 \times 10^{20}$ cm^{-2} (<1.6×10^{22} cm^{-2} at 90% confidence). In contrast to NGC 720, NGC 4552 has a noisy spectrum between 0.2 and 1 keV. NGC 4552 is a pointlike source and it is ~10′ away from the IPC center. There is no nearby source and its background spectrum look smooth suggesting that the spectral features are indeed associated with the galaxy. The spectrum of NGC 4151 is described below.

2.2. *Elliptical and Spiral Galaxies*

Figures 5*a* and 5*b* show the 68% and 90% allowed kT for elliptical and spiral galaxies, respectively. While the uncertainties are very large in most cases, these figures show a concentra-

1992ApJS...80..645K

TABLE 1

X-RAY SPECTRAL PROPERTIES OF ELLIPTICAL GALAXIES: FIT TO A THERMAL SPECTRUM

name	type (T)		RA (1950) (h m s)	Dec (1950) (° ′ ″)	Seq	Exp. (sec)	Source radius (″)	Background radii (″)		Off ang (′)	Counts	Error	Gain	PH	En. range (keV)	Best Fit (and 90%) Parameters kT (keV)			log N$_H$ (cm^{-2})			logN$_H$ (Gal.) (cm^{-2})	χ^2	D
N0499	-3		1 20 22	+33 12 00	7766	9193.4	210	400	600	11.00	811.3	34.9	16.11	2-12	.1- 5.0	0.9	(0.5	- 1.4)	21.8	(20.8	- 22.1)	20.7	5.5	8
N0507	-2		1 20 50	+32 59 42	7766	9193.4	630	700	900	5.84	2937.5	87.0	14.94	2-11	.2- 4.6	3.1	(1.6	-)	21.1	(20.9	- 21.5)	20.7	3.3	7
N0720	-5		1 50 34	-13 59 05	5769	4477.1	480	600	800	0.28	417.7	36.0	16.42	2-12	.1- 4.8	0.1	(	-)	21.5	(	- 21.9)	20.2	22.1	8
N1316	-2		3 20 47	-37 23 06	1884	4840.9	450	540	660	2.36	330.8	34.9	12.58	2-9	.3- 4.0	0.5	(	- 1.2)	19.0	(	- 22.2)	20.3	9.8	5
N1332	-2		3 24 04	-21 30 30	7028	12498.6	360	420	540	0.09	314.3	46.5	16.48	2-12	.1- 4.7	4.3	(0.4	-)	19.9	(	- 22.2)	20.4	1.8	8
N1395	-5		3 36 19	-23 11 23	9185	13922.2	480	540	660	0.51	902.2	115.4	17.51	2-13	.1- 5.3	1.6	(	-)	20.2	(	- 22.5)	20.2	3.2	9
N1399	-5	a	3 36 35	-35 36 42	1887	3657.9	1200	1210	1300	4.71	2881.5	216.3	16.49	2-12	.1- 4.7	2.0	(1.1	-)	20.5	(19.7	- 21.4)	20.1	6.8	8
N1404	-5	a	3 36 57	-35 45 17	1887	3657.9	300	360	480	12.45	431.7	43.8	18.04	2-13	.1- 4.9	2.0	(0.8	-)	20.2	(	- 22.1)	20.1	9.2	9
N3607	-2		11 14 17	+18 19 42	3927	16041.9	300	420	540	0.21	385.5	39.2	12.40	2-10	.3- 5.3	1.2	(0.4	-)	19.0	(	- 22.0)	20.2	11.8	6
N4291	-5		12 18 07	+75 38 47	5424	13112.9	270	300	500	6.53	409.6	34.7	16.48	2-12	.1- 4.7	4.3	(0.4	-)	21.1	(20.7	- 22.1)	20.5	5.0	8
N4374	-5	b	12 22 31	+13 09 48	278	34963.8	300	330	420	23.54	1527.6	109.1	15.51	2-11	.2- 4.2	1.6	(0.8	-)	20.2	(19.5	- 21.6)	20.4	10.8	7
N4406	-3		12 23 40	+13 13 23	4311	4558.2	840	860	990	0.89	3102.4	117.0	18.11	3-13	.2- 4.8	1.2	(1.1	- 2.1)	20.5	(20.1	- 21.1)	20.4	10.5	8
N4472	-3		12 27 14	+08 16 42	4308 c	7672.2	810	820	900	0.66	3853.7	136.1	14.81	2-11	.2- 4.7	1.2	(1.1	- 1.9)	20.5	(20.1	- 21.0)	20.2	11.8	7
N4552	-2		12 33 08	+12 50 00	4313	8426.0	150	300	500	9.81	280.8	21.0	18.30	3-13	.2- 4.7	0.9	(	- 1.6)	21.1	(19.8	- 22.5)	20.4	19.6	8
N4636	-3		12 40 17	+02 57 42	412	1383.9	600	630	690	0.28	644.6	52.2	16.79	2-12	.1- 4.5	0.9	(0.5	- 1.8)	20.5	(19.2	- 22.0)	20.3	6.4	8
N4649	-2		12 41 09	+11 49 30	2130	6160.6	420	450	550	0.69	1142.5	55.2	16.46	2-12	.1- 4.7	1.6	(0.4	- 3.1)	20.8	(20.4	- 22.1)	20.4	5.5	8
N4756	-5		12 50 15	-15 08 36	1900 c	5511.2	270	920	1100	3.70	302.0	25.6	17.54	2-13	.1- 5.3	1.2	(0.7	-)	19.6	(	- 20.6)	20.5	2.1	9
N5044	-5	a	13 12 44	-16 07 18	6653	1389.6	780	1000	1200	0.95	1408.7	59.8	16.38	2-11	.1- 3.8	1.2	(0.8	- 1.6)	20.8	(20.4	- 21.7)	20.7	5.0	7
I4296	-5		13 33 47	-33 42 24	1902	10592.7	360	420	540	12.70	320.3	44.4	14.66	2-11	.2- 4.8	1.2	(	-)	20.8	(19.3	- 22.7)	20.6	3.4	7
N5846	-2		15 03 56	+01 47 47	9975	14344.0	600	630	720	0.21	3000.0	123.9	17.84	2-12	.1- 3.9	1.2	(1.0	- 1.9)	20.2	(19.9	- 20.6)	20.6	13.5	8
N7619	-5		23 17 43	+07 56 00	2598	8757.0	300	600	800	9.67	418.8	31.5	12.49	2-10	.3- 5.2	0.1	(	- 1.1)	22.4	(20.8	- 22.6)	20.7	7.5	6

[a] X-ray emission may be contaminated by the intracluster emission.
[b] NGC 4374 is outside the ribs.
[c] Gain change is larger than 10% (see text).

1992ApJS...80..645K

TABLE 2

X-RAY SPECTRAL PROPERTIES OF SPIRAL GALAXIES: FIT TO A THERMAL SPECTRUM

name	type (T)	RA (1950) (h m s)	Dec (1950) (° ′ ″)	Seq	Exp. (sec)	Source radius (″)	Background radii (″)	Off ang (′)	Counts	Error	Gain	PH	En. range (keV)	Best Fit (and 90%) Parameters kT (keV)	log N_H (cm^{-2})	logN_H (Gal.) (cm^{-2})	χ^2	D
N0247	5	0 44 40	-21 02 00	5766	10225.0	600	630 720	2.47	645.7	88.6	12.30	2-10	.3- 5.4	5.0 (0.5 -)	19.6 (- 21.8)	20.2	10.3	6
N0253	5	0 45 08	-25 33 42	2082	7762.6	660	690 780	0.39	2309.7	96.6	18.31	2-13	.1- 4.7	5.0 (2.3 -)	19.9 (19.4 - 20.3)	20.1	13.6	9
N1097	4	2 44 11	-30 29 06	2093 a	5314.9	210	330 420	1.80	476.6	25.1	12.85	2-10	.2- 4.9	1.6 (0.8 -)	20.5 (19.3 - 21.2)	20.3	3.5	6
N1313	5	3 17 39	-66 40 42	7044	7775.1	180	300 420	0.57	405.1	23.8	18.47	2-12	.1- 3.6	1.2 (0.5 -)	21.8 (21.1 - 22.1)	20.5	8.0	8
N2403	5	7 32 03	+65 42 42	589	5988.3	390	420 540	0.39	321.6	34.1	15.12	2-11	.2- 4.5	5.0 (1.2 -)	20.5 (- 21.6)	20.6	9.8	7
N3031	3	9 51 30	+69 18 17	2102	6515.2	480	500 600	0.89	1634.8	66.2	17.53	2-12	.1- 4.1	0.5 (0.4 - 0.9)	21.5 (20.8 - 21.6)	20.6	8.9	8
N3034	0	9 51 41	+69 54 54	466	4449.8	660	700 900	0.21	2879.1	71.3	16.51	2-12	.1- 4.7	3.1 (1.2 - 4.8)	21.1 (21.1 - 21.5)	20.6	10.1	8
N3628	4	11 17 40	+13 52 05	5152	12680.4	390	450 600	0.34	735.5	48.2	12.84	2-10	.2- 4.9	5.0 (1.5 -)	21.5 (21.2 - 22.0)	20.3	8.7	6
N4388	2	12 23 14	+12 56 17	278	34963.8	210	240 360	11.26	713.8	60.3	13.92	2-11	.2- 5.4	1.2 (0.5 -)	21.2 (20.1 - 21.8)	20.4	14.1	7
N4501	4	12 29 28	+14 41 42	4304	10272.0	240	400 500	0.74	300.3	32.9	15.78	2-12	.1- 5.3	3.5 (0.7 -)	19.9 (- 21.1)	20.4	14.2	8
N4565	3	12 33 52	+26 15 36	9974	20694.6	300	500 700	7.00	484.3	39.4	11.84	2-10	.3- 5.8	1.2 (0.5 -)	21.5 (20.2 - 22.1)	20.1	13.1	6
N4579	2	12 35 12	+12 05 35	4315	7290.0	270	420 600	0.74	1680.8	47.2	15.99	2-12	.1- 5.1	3.1 (1.6 -)	20.8 (20.7 - 21.1)	20.4	5.1	8
N4594	2	12 37 23	-11 21 00	2127	5282.2	390	500 600	0.39	458.6	35.5	13.97	2-11	.2- 5.4	2.0 (0.5 -)	21.1 (20.3 - 21.9)	20.6	3.4	7
N5236	5	13 34 10	-29 36 47	588 a	5708.1	390	500 630	0.81	759.5	38.6	13.94	2-10	.2- 4.2	2.0 (1.0 -)	20.5 (19.7 - 20.9)	20.6	4.0	6
N6744	4	19 05 02	-63 56 17	7063	20546.1	240	420 540	1.27	416.3	38.2	13.96	2-10	.2- 4.2	0.5 (0.5 -)	22.1 (20.8 - 22.2)	20.8	5.6	6
N6946	5	20 33 48	+59 59 00	10314	20871.7	480	600 700	1.83	1571.3	98.4	14.12	2-10	.2- 4.1	4.6 (0.8 -)	21.1 (20.6 - 21.8)	21.3	4.9	6
N6946	5	20 33 48	+59 59 00	10597	7444.1	480	600 700	2.08	610.7	60.4	17.89	2-13	.1- 5.0	3.9 (0.4 -)	21.1 (20.5 - 22.2)	21.3	11.1	9

[a] Gain change is larger than 10% (see text).

1992ApJS...80..645K

TABLE 3

X-RAY SPECTRAL PROPERTIES OF ACTIVE GALACTIC NUCLEI FIT TO A POWER-LAW SPECTRUM

name	type (T)	RA (1950) (h m s)	Dec (1950) (° ′ ″)	Seq	Exp. (sec)	Source radius (″)	Background radii (″)	Off ang (″)	Counts	Error	Gain	PH	E (keV)	Best Fit (and 90%) Parameters kT (keV)	log N_H (cm^{-2})	logN_H (Gal.) (cm^{-2})	χ^2	D	
N0315	-3	0 55 05	+30 04 54	4374	17433.8	300	360 480	0.09	581.1	43.4	12.31	2-10	.3- 5.4	2.5 (1.1 -)	21.5 (20.2 - 22.1)	20.8	4.4	6	
N0985	10	2 32 11	-09 00 18	3143	3302.8	450	540 660	0.21	1874.1	49.9	16.35	2-11	.1- 3.8	1.3 (1.2 - 1.5)	19.5 (- 20.1)	20.5	10.0	7	
N4051	4	12 00 37	+44 48 42	7200 a	8796.6	480	600 720	0.69	6657.8	97.5	16.66	2-12	.1- 4.6	1.9 (1.8 - 2.1)	19.3 (- 19.9)	20.1	6.9	8	
N4151	2	12 08 00	+39 40 54	352	6901.0	360	720 820	1.10	2172.2	52.0	17.24	2-12	.1- 4.3	0.8 (0.6 - 0.9)	19.0 (- 19.7)	20.3	33.6	8	b
N4151	2	12 08 00	+39 40 54	353 a	19928.5	360	720 820	1.28	5942.4	85.8	15.29	2-11	.2- 4.4	0.8 (0.7 - 0.9)	19.0 (- 19.7)	20.3	30.6	7	b
N4261	-5	12 16 50	+06 06 05	6309	6905.9	330	360 480	0.85	321.1	35.7	14.26	2-10	.2- 4.0	3.7 (1.4 -)	21.5 (19.7 - 21.9)	20.2	5.5	6	
N5548	1	14 15 43	+25 22 00	356	22397.2	600	1000 1200	0.34	25954.0	465.3	17.86	2-13	.1- 5.0	1.3 (1.2 - 1.5)	19.3 (- 20.0)	20.2	8.1	9	

[a] Gain change is larger than 10% (see text).

[b] A two-component model is shown in Fig. 7 (see also text).

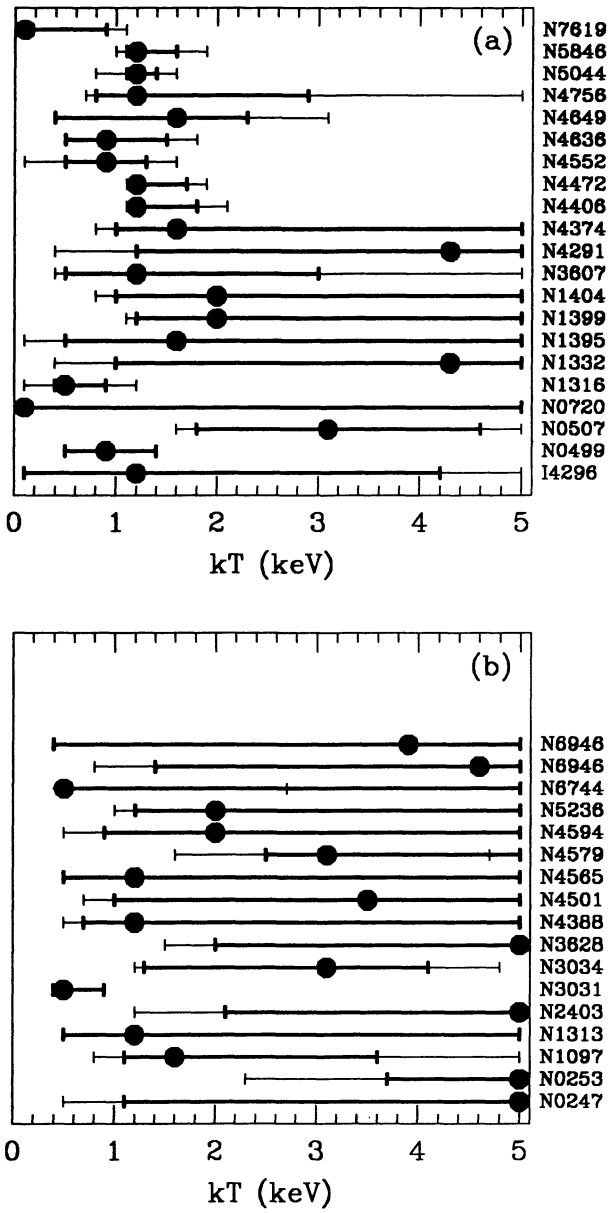

FIG. 5.—Range of allowed kT for (a) elliptical and (b) spiral galaxies. The filled circle is the best-fit value, the thick line is the allowed range at 68% confidence and the thin line is the range at 90% confidence.

tion of the kT of elliptical galaxies around 1–1.5 keV. One noticeable exception is NGC 507. NGC 507 is the dominant galaxy in a group and the higher kT could reflect the presence of a deeper potential well. Its X-ray emission may include a component from intracluster emission. On the other hand, spiral galaxies have a much broader range of kT and suggest higher emission temperatures. A clear exception is NGC 3031 (M81), whose X-ray emission is however dominated by an active nucleus (see Fabbiano 1988a). Detailed comparisons of emission temperatures in ellipticals and spirals and their implications on the emission mechanisms are described in Paper III.

Figures 6a and 6b show the allowed N_H of elliptical and spiral galaxies, respectively, compared with the line-of-sight Galactic N_H (Stark et al. 1992). In most instances, the N_H from the spectral fits is consistent (within error) with the Galactic N_H. There are however cases, both in early- and late-type galaxies, where the X-ray spectrum indicates a significant amount of internal absorption.

Spiral galaxies with N_H in excess of the Galactic value are NGC 1313, NGC 3031 (M81), NGC 3034 (M82), NGC 3628, NGC 4565, and NGC 4579. The first two may contain a small AGN (Fabbiano & Trinchieri 1987; Fabbiano 1988a). M82 and NGC 3628 have starburst nuclei with evidence of large optical depth (see also Fabbiano 1988b and Fabbiano, Heckman, & Keel 1990). NGC 4565 is an edge-on galaxy with an optically prominent dust lane. NGC 4579 contains a low-luminosity active nucleus (Filippenko & Sargent 1985) and its radial profile of X-ray surface brightness is pointlike (see Paper I).

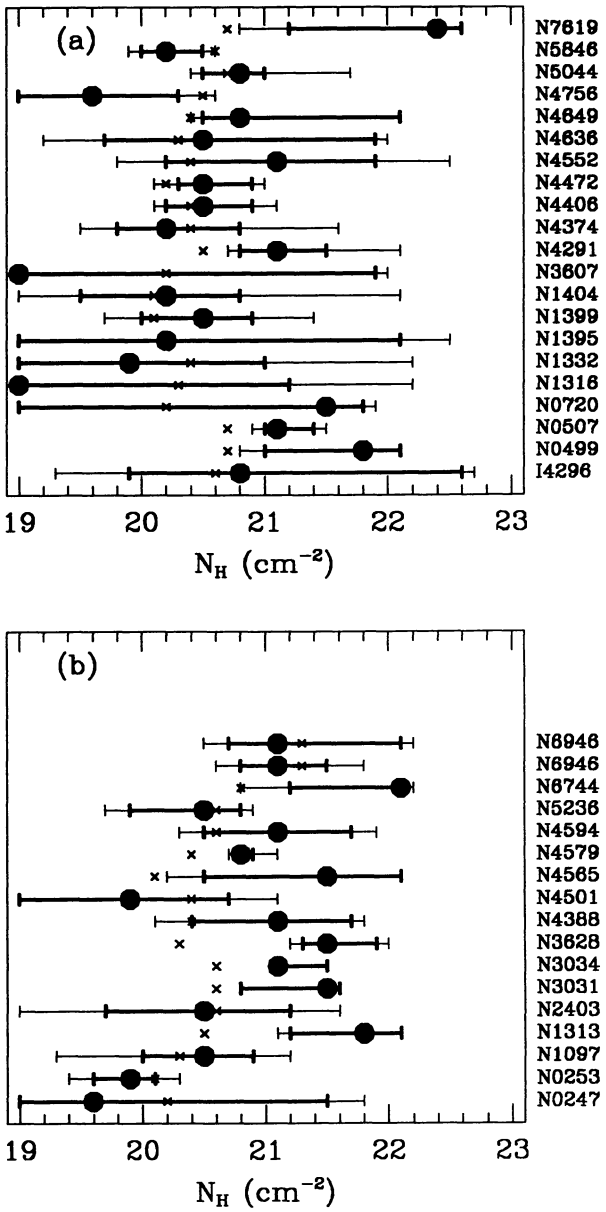

FIG. 6.—Same as Fig. 5 but for the range of allowed N_H. The cross (×) identifies the Galactic line-of-sight N_H.

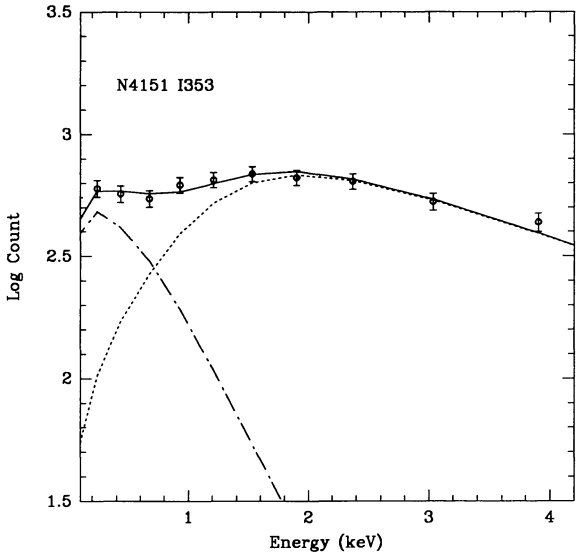

FIG. 7.—Spectral fit of NGC 4151 to a two-component model. The dotted line is a power-law model prediction with $\alpha = -0.19$ and the dot-dashed line is a thermal model prediction with $kT = 0.17$ keV. The H I column density is fixed at the Galactic value (2.1×10^{20} cm^{-2}). The solid line is a sum of the two model predictions.

More surprising is the presence of intrinsic N_H in elliptical galaxies, which do not have amounts of dense interstellar matter comparable to those of spirals (for example, Schweizer 1987). This effect was first noticed in NGC 4472 and NGC 4649 by Trinchieri et al. (1986), who suggested that this could be due to a larger than solar metallicity of the X-ray emitting gas, instead of being a genuine absorption effect. The X-ray derived N_H is significantly larger than the Galactic value in NGC 499, NGC 507, NGC 4291, and NGC 7619. NGC 4291 and NGC 7619 have nearby X-ray sources (Mkn 205 and NGC 7626, respectively), which might contaminate the X-ray emission of these galaxies (their X-ray spectra look noisy in Fig. 2). NGC 499 and NGC 507 are also close to each other. However, even if their spectra are contaminated by the other galaxy's emission, their intrinsic absorption are likely real because both galaxies have large N_H and their spectra are smooth (see Fig. 2). If these large cutoffs are indeed due to absorption, they may be indicative of substantial amounts of cold matter, possibly connected with cooling flows (A. Fabian 1991, private communication). These galaxies will be discussed in a separate paper (Kim, Fabbiano, & Eskridge 1992).

2.3. *Active Galactic Nuclei*

There are 17 galaxies in our sample which host strong AGNs. We have fitted these spectra with a power-law model as described above. Most of these 17 AGNs are in the sample of KUC and our results are comparable with theirs. We will not discuss these galaxies further. In Table 3 and Figure 4 we show our results for three galaxies not included in KUC (NGC 315, NGC 4051, and NGC 4261). We also include the observations of NGC 4151 and NGC 5548. These were analyzed by KUC, who, however, do not list spectral parameters nor show spectral confidence contours because they obtained very bad fits ($\chi^2 = 108.9$ for 11 degrees of freedom and $\chi^2 = 108.4$ for 10 degrees of freedom, respectively). Given the very high signal-to-noise ratio of these observations we have fitted these data using a much finer grid than in KUC. We still do not find an acceptable fit for NGC 4151, but we obtained an acceptable fit

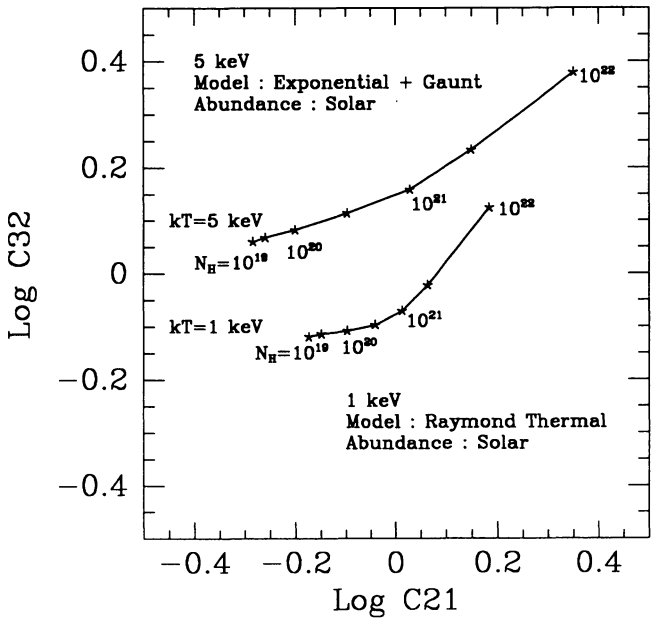

FIG. 8a

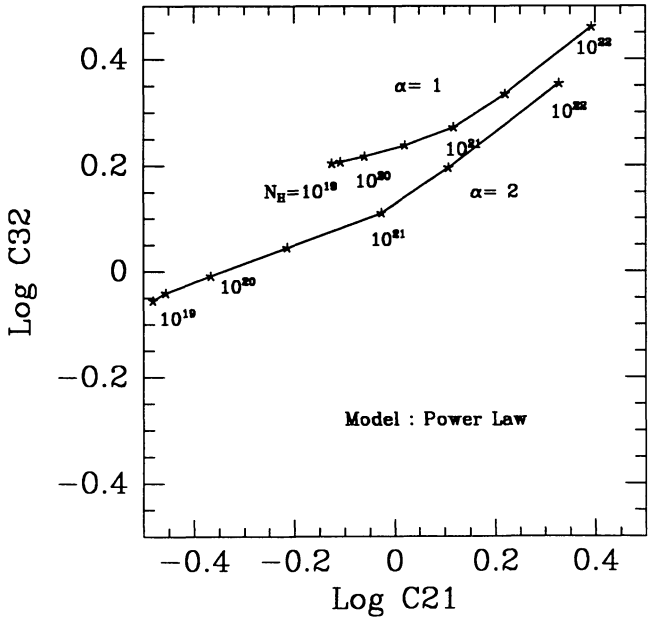

FIG. 8b

FIG. 8.—X-ray color-color plot. (*a*) The lower line is for Raymond thermal emission with lines at 1 keV and the upper line is for Bremsstrahlung emission at 5 keV with varying N_H. In the thermal model, solar abundance is used. (*b*) Power-law model predictions. The upper line is with photon index $\alpha = 2$ and the lower line is with $\alpha = 1$.

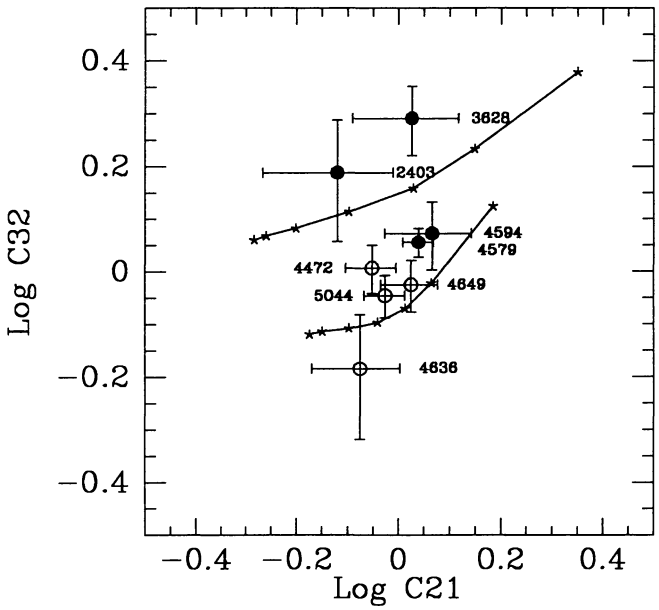

FIG. 9a

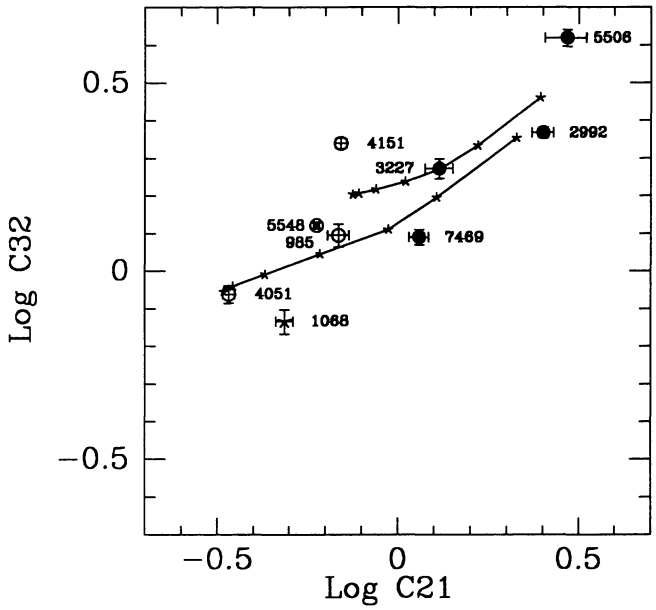

FIG. 9b

FIG. 9.—(*a*) X-ray colors for elliptical (*open circles*) and spiral (*filled circles*) galaxies. Lines are the same as in Fig. 8. (*b*) X-ray colors for AGNs.

for NGC 5548. Furthermore, we include NGC 985 in Table 3 and Figure 4. For this galaxy, KUC also obtained a χ^2 significantly higher than the one we obtain when we do a fit with a finer grid. In NGC 985, NGC 4051, NGC 4151, and NGC 5548 we find very clear evidence of soft components and/or complex spectra as evidenced by N_H significantly below the galactic N_H (see also KUC).

In the case of NGC 4151 we also show a two component fit in Figure 7. This fit gives an acceptable $\chi^2 = 3.7$ for 7 degrees of freedom. The solid line is a sum of a power-law model with $\alpha = -0.19$ (*dotted line*) and a thermal model with $kT = 0.17$ keV (*dot-dashed line*). In both models, N_H is fixed at the Galactic value (2.1×10^{20} cm^{-2}). The addition of a relatively small contribution (~25%) of a very soft component could, therefore, reproduce the observed spectrum of NGC 4151. This soft component can be seen clearly in the *EXOSAT* spectrum of NGC 4151 (Pounds et al. 1986). A similar trend has also been found in some quasars (Wilkes & Elvis 1987).

3. X-RAY COLORS

Often galaxies detected with the *Einstein* Observatory do not have enough counts for us to use the standard model fitting technique. In this case one would wish to use a different method to infer some spectral information. One method would be to use the hardness ratio calculated by the Rev 1B IPC processing (Harnden et al. 1984) by using two energy bands (soft and hard bands). However, with this ratio we cannot determine two spectral parameters, unless there is a priori information to fix one of them. Since, as shown in § 2, the soft band is strongly affected by varying absorption column densities, the hardness ratio alone cannot give unique estimates of the intrinsic spectral parameters. Therefore, to obtain an estimate of both the emission temperature (kT) or power-law index (α) and line-of-sight H I column density (N_H), we have used two X-ray colors, defined as

$$\text{C21} = \text{counts}(0.8\text{–}1.4\text{keV})/\text{counts}(0.2\text{–}0.8\text{keV}),$$

$$\text{C32} = \text{counts}(1.4\text{–}3.5\text{keV})/\text{counts}(0.8\text{–}1.4\text{keV}).$$

The energy boundaries of the two colors were chosen so that each band has similar counts to minimize the resulting errors in the estimate of the X-ray color. In order to fix the energy ranges, we have used PI bins (pulse height invariant bin) because the energy range of each PH bin (pulse height, used in the standard model fitting) depends on the gain of each observation. For details of PI bins, we refer to Harnden et al. (1984).

In Figure 8*a*, we plot the X-ray colors predicted by the thermal models (for 1 keV, we use the Raymond thermal model with emission lines and for 5 keV, the Bremsstrahlung model). At high temperatures (~5 keV), the two models produce almost similar results. In the Raymond thermal model, solar abundance was assumed. Within a reasonable parameter range ($kT = 1$ to 5 keV and $N_H = 10^{19}$ to 10^{22} cm^{-2}), the first X-ray color (C21) is sensitive primarily to the hydrogen column density N_H, while the second color (C32) is sensitive to the emission temperature except for very large column densities. For large absorbing column densities ($N_H \sim 10^{22}$ cm^{-2}), a 1 keV spectrum looks hard due to strong absorption even above 0.8 keV. In Figure 8*b*, we plot the X-ray colors predicted by the power-law model, for $\alpha = 1$ and 2 (photon index).

In order to establish the reliability of this method, we have compared the X-ray colors with the results of the standard fitting of § 2. We first plot colors of galaxies with well-determined spectral parameters (Fig. 9*a*). Each galaxy is labeled by its NGC name and error bars are 1 σ statistical errors. Within the uncertainties, the column densities and temperatures estimated by the χ^2 fit (see § 2) are consistent with the locations of the galaxies in the color-color diagram. Elliptical galaxies

TABLE 4

X-RAY COLORS

Name	Type (T)		RA (1950) (h m s)	Dec (1950) (d ' ")	Seq	Exp. (sec)	Source radius (")	background radii (")		Counts	Error	C21	Error	C32	Error	
N0247	5		0 44 40	-21 02 00	5766	10225.05	600	630	720	537.16	83.27	0.342	0.141	1.273	0.620	
N0253	5		0 45 08	-25 33 42	2082	7762.58	660	690	780	1941.57	92.20	0.574	0.066	1.288	0.155	
N0315	-3	a	0 55 05	+30 04 54	c					639.99	41.08	1.119	0.192	1.241	0.172	
N0499	-3		1 20 22	+33 12 00	7766	9193.43	210	400	600	913.71	38.32	1.175	0.126	1.104	0.107	d
N0507	-2		1 20 50	+32 59 42	7766	9193.43	630	700	900	2636.13	93.50	1.527	0.184	1.527	0.110	
N0524	0		1 22 10	+09 16 42	2089	5754.58	240	360	480	110.29	17.41	0.999	0.389	0.954	0.347	
N0628	5		1 34 01	+15 31 36	7042	6650.73	300	360	480	74.29	21.69	0.794	0.474	0.684	0.566	
N0720	-5		1 50 34	-13 59 05	5769	4477.13	480	600	800	305.94	34.83	0.353	0.098	0.922	0.373	
N0936	0		2 25 05	-01 22 42	c					171.00	37.49	1.215	1.017	1.191	0.579	
N0985	10	a	2 32 11	-09 00 18	3143	3302.79	450	540	660	1791.10	48.45	0.686	0.046	1.246	0.087	
N1042	5		2 37 56	-08 38 47	1880	10928.29	240	360	480	189.26	26.96	0.956	0.342	1.147	0.354	d
N1052	-3		2 38 37	-08 28 06	1880	10928.29	240	360	480	211.79	25.41	1.106	0.371	1.308	0.337	
N1068	3	a	2 40 07	-00 13 30	c					2179.75	51.60	0.487	0.027	0.735	0.055	
N1097	4		2 44 11	-30 29 06	2093	5314.87	210	330	420	488.51	25.74	0.838	0.107	1.080	0.137	
N1218	0	a	3 05 49	+03 55 12	9146	1467.67	210	360	540	83.21	10.77	1.827	0.775	1.441	0.396	
N1313	5		3 17 39	-66 40 42	7044	7775.14	180	300	420	405.80	23.65	1.207	0.201	1.500	0.195	
N1316	-2		3 20 47	-37 23 06	c					877.03	58.90	0.568	0.084	0.723	0.152	
N1332	-2		3 24 04	-21 30 30	7028	12498.61	360	420	540	325.19	39.86	0.809	0.258	1.364	0.360	
N1365	3		3 31 42	-36 18 17	c					206.02	24.02	0.630	0.180	1.209	0.367	
N1380	0		3 34 31	-35 08 23	5777	1584.98	210	270	480	37.16	9.59	0.557	0.423	2.171	1.489	
N1386	1		3 34 52	-36 09 53	4129	3312.75	180	240	360	49.30	13.57	0.453	0.263	0.390	0.517	d
N1395	-5		3 36 19	-23 11 23	9185	13922.24	480	540	660	764.89	84.11	0.859	0.238	1.009	0.228	
N1399	-5	b	3 36 35	-35 36 42	1887	3657.91	1200	1210	1300	2535.34	197.14	0.933	0.191	1.233	0.211	
N1398	2		3 36 45	-26 29 53	c					174.96	20.61	0.535	0.143	0.959	0.373	
N1404	-5		3 36 57	-35 45 17	1887	3657.91	300	360	480	494.26	36.07	0.850	0.145	0.935	0.169	d
N1407	-5		3 37 57	-18 44 24	10241	4230.77	300	320	400	248.98	24.18	0.747	0.179	1.270	0.290	
I0342	6		3 41 57	+67 56 24	7045	2059.18	510	540	660	189.71	29.25	0.912	0.473	2.343	0.832	
N1533	0		4 08 50	-56 15 00	7030	10378.52	240	360	420	106.16	25.86	0.321	0.216	1.513	1.186	
N1559	5		4 17 01	-62 54 17	7046	8378.34	180	360	480	227.93	21.03	0.784	0.204	1.808	0.391	
N1566	5	a	4 18 53	-55 03 24	c					1261.59	40.67	0.666	0.054	1.206	0.098	
N1569	9		4 26 05	+64 44 24	414	2847.17	210	400	500	99.84	12.70	0.832	0.309	2.105	0.656	
N1672	3		4 44 58	-59 19 36	427	5800.66	210	360	480	135.82	18.09	0.573	0.205	1.664	0.551	
N1784	4		5 03 07	-11 56 24	10225	14314.05	150	420	580	63.43	15.85	1.048	0.561	0.481	0.349	
N1961	3		5 36 34	+69 21 17	9460	10236.66	180	400	600	80.84	16.15	0.613	0.279	1.035	0.525	
N2403	5		7 32 03	+65 42 42	c					572.39	50.24	0.749	0.202	2.119	0.513	
N2563	-2		8 17 40	+21 13 36	304	8858.54	360	600	900	276.15	35.35	0.724	0.191	0.579	0.231	
N2775	1		9 07 41	+07 14 30	7048	6080.11	180	360	480	76.83	14.14	0.986	0.427	0.850	0.363	
N2832	-5	b	9 16 45	+33 57 35	1841	1550.59	360	420	540	126.97	20.34	0.568	0.243	1.527	0.619	
N2841	3		9 18 35	+51 11 18	2099	4907.66	180	360	480	79.91	12.88	0.466	0.204	1.690	0.730	
N2903	5		9 29 20	+21 43 12	7049	4369.10	210	360	480	175.59	17.11	0.635	0.154	1.349	0.322	
N2992	1	a	9 43 18	-14 05 41	c					5418.06	82.91	2.522	0.174	2.336	0.079	
N3031	3		9 51 30	+69 18 17	2102	6515.22	480	500	600	1585.31	62.19	0.866	0.075	0.753	0.076	
N3034	0		9 51 41	+69 54 54	466	4449.77	660	700	900	2594.93	71.56	1.180	0.089	1.261	0.075	
N3078	-5		9 56 08	-26 41 12	10242	5476.82	210	240	360	77.47	16.07	1.140	0.577	0.829	0.387	
N3081	1		9 57 11	-22 35 05	5251	1640.56	180	450	600	38.21	7.92	0.581	0.288	1.139	0.608	
N3227	3	a	10 20 47	+20 07 05	c					2374.98	58.58	1.302	0.115	1.874	0.113	
N3310	4		10 35 39	+53 45 54	467	1389.18	150	240	330	49.79	8.21	1.221	0.522	1.141	0.429	
N3395	5		10 47 02	+33 14 41	3936	5422.19	180	400	500	61.33	15.45	1.089	0.712	1.086	0.587	d
N3516	-2	a	11 03 23	+72 50 24	c					731.24	34.96	0.927	0.129	1.977	0.217	
N3607	-2		11 14 17	+18 19 42	3927	16041.83	300	420	540	382.51	41.51	1.003	0.242	0.530	0.148	
N3628	4		11 17 40	+13 52 05	5152	12680.45	390	450	600	683.27	48.92	1.062	0.249	1.955	0.294	
N3660	4	a	11 21 06	-08 24 00	10228	5606.30	330	420	540	196.31	27.11	0.800	0.275	1.166	0.349	
N3783	1	a	11 36 33	-37 27 42	7209	7442.23	690	700	800	6735.09	119.64	1.386	0.077	1.598	0.059	
N3923	-3		11 48 30	-28 31 42	5800	4464.59	270	360	480	166.62	19.65	0.739	0.198	0.861	0.258	
N3998	-2	a	11 55 20	+55 44 05	4548	1281.99	330	360	480	309.01	21.85	0.800	0.150	1.516	0.250	
N4038	5		11 59 19	-18 35 05	c					263.43	21.92	0.849	0.172	1.051	0.219	
N4051	4	a	12 00 37	+44 48 42	7200	8796.61	480	600	720	5903.91	93.28	0.341	0.013	0.868	0.047	
N4151	2	a	12 08 00	+39 40 54	c					7434.52	97.87	0.697	0.026	2.190	0.073	
N4156	3		12 08 17	+39 44 54	c					404.73	29.82	0.680	0.141	1.701	0.315	
N4168	-5		12 09 44	+13 29 00	6974	5108.55	180	330	450	62.70	12.11	1.039	0.547	1.195	0.485	
N4192	3		12 11 15	+15 10 48	6978	6504.59	150	240	330	33.22	12.34	0.530	0.405	0.641	0.779	

TABLE 4—*Continued*

Name	Type (T)		RA (1950) (h m s)	Dec (1950) (d ' ")	Seq	Exp. (sec)	Source radius (")	background radii (")		Counts	Error	C21	Error	C32	Error	
N4203	-2		12 12 34	+33 28 42	3922	1543.60	240	360	480	183.10	16.51	0.515	0.117	1.441	0.331	
N4235	1	a	12 14 37	+07 28 06	6711	2132.81	150	330	480	260.72	17.51	1.569	0.302	1.162	0.170	
N4254	5		12 16 17	+14 41 42	4306	10781.03	150	240	360	129.77	17.49	0.692	0.215	0.968	0.316	
N4261	-5	a	12 16 50	+06 06 05	c					443.14	42.38	0.746	0.179	1.384	0.446	
N4291	-5		12 18 07	+75 38 47	5424	13112.91	270	300	500	390.72	34.53	0.877	0.183	0.971	0.205	
N4298	5		12 19 00	+14 53 05	4305	14918.96	240	300	400	124.69	30.31	0.961	0.527	0.736	0.432	
N4303	5		12 19 22	+04 45 05	c					344.29	28.83	0.545	0.103	0.892	0.198	
N4321	5		12 20 23	+16 06 00	4301	1914.36	210	240	360	52.08	11.01	1.018	0.552	1.166	0.509	
N4365	-5		12 21 56	+07 35 42	c					115.81	15.45	0.971	0.340	0.909	0.283	
N4374	-5		12 22 31	+13 09 48	c					3081.98	129.17	0.858	0.087	1.063	0.108	
N4382	-2		12 22 53	+18 28 00	c					425.46	39.15	0.455	0.106	1.428	0.370	
N4388	2		12 23 14	+12 56 17	278	34963.81	210	240	360	767.23	61.77	0.909	0.168	0.802	0.162	d
N4406	-3		12 23 40	+13 13 23	4311	4558.25	840	860	990	2592.53	143.00	1.113	0.151	0.865	0.108	
N4449	9		12 25 47	+44 22 17	2123	1612.26	180	400	600	64.90	9.52	0.692	0.241	1.042	0.386	
N4450	2		12 25 59	+17 21 42	7001	3255.96	270	360	480	105.59	17.50	0.505	0.203	1.239	0.541	
N4472	-3		12 27 14	+08 16 42	4308	7672.18	810	820	900	3397.16	158.21	0.888	0.100	1.016	0.108	
N4477	0		12 27 31	+13 54 42	c					486.10	62.70	0.706	0.179	0.549	0.280	
N4501	4		12 29 28	+14 41 42	4304	10271.97	240	400	500	283.33	31.35	0.565	0.151	1.152	0.348	
N4526	-2		12 31 31	+07 58 30	4309	8388.77	180	240	360	71.91	17.62	0.792	0.433	0.786	0.443	
N4536	5		12 31 54	+02 27 42	9134	3688.28	210	600	700	68.08	14.42	1.021	0.582	1.107	0.476	
I3528	3		12 32 25	+15 50 30	7795	1728.75	180	240	360	127.95	18.98	0.663	0.233	0.945	0.375	d
N4552	-2		12 33 08	+12 50 00	4313	8426.00	150	300	500	317.44	23.42	0.808	0.130	0.615	0.128	d
N4565	3		12 33 52	+26 15 36	9974	20694.65	300	500	700	551.20	43.58	1.079	0.216	0.971	0.165	
N4567	5		12 34 01	+11 32 00	4317	5456.10	210	240	360	87.47	19.37	0.224	0.180	1.812	1.656	
N4579	2		12 35 12	+12 05 35	c					1833.46	49.11	1.094	0.075	1.137	0.071	
N4594	2		12 37 23	-11 21 00	c					569.93	38.99	1.163	0.222	1.182	0.174	
N4631	5		12 39 41	+32 48 47	471	3047.58	270	420	560	135.25	16.47	1.117	0.329	0.818	0.229	
N4636	-3		12 40 17	+02 57 42	412	1383.87	600	630	690	566.50	53.54	0.841	0.164	0.654	0.174	
N4639	3		12 40 21	+13 31 53	c					349.00	34.94	1.145	0.420	1.127	0.261	
N4649	-2		12 41 09	+11 49 30	2130	6160.56	420	450	550	1035.41	52.47	1.058	0.134	0.944	0.107	
N4689	5		12 45 15	+14 02 05	7018	4297.08	150	270	400	112.85	13.27	0.602	0.196	1.994	0.583	
N4697	-5		12 46 01	-05 31 42	c					179.33	29.43	0.671	0.260	0.831	0.366	
N4756	-5		12 50 15	-15 08 36	1900	5511.29	270	920	100	172.47	22.96	0.993	0.321	0.942	0.291	
N4826	2		12 54 17	+21 57 05	2136	4867.41	270	360	480	116.36	19.53	0.391	0.142	0.571	0.407	
N4861	9		12 56 40	+35 07 54	445	2604.70	300	360	480	58.04	15.79	0.956	0.889	2.124	1.181	
N5044	-5	b	13 12 44	-16 07 18	6653	1389.62	780	1000	1200	1457.07	55.76	0.942	0.086	0.900	0.083	
N5077	-5		13 16 53	-12 23 42	10244	6140.50	120	420	540	53.46	10.18	0.654	0.264	0.528	0.326	
N5128	-2	a	13 22 32	-42 45 30	477	12473.02	1020	1100	1300	15461.60	212.76	1.232	0.108	5.745	0.267	
N5204	7		13 27 44	+58 40 42	7635	6975.38	150	240	400	199.26	17.84	1.290	0.314	1.080	0.209	
I4296	-5		13 33 47	-33 42 24	1902	10592.73	360	420	540	407.13	53.59	1.666	0.690	0.900	0.225	d
N5236	5		13 34 10	-29 36 47	588	5708.12	390	500	630	772.95	38.80	0.884	0.105	0.917	0.111	
N5248	4		13 35 03	+09 08 30	9136	3639.61	120	240	360	33.77	8.58	1.902	1.214	0.307	0.245	
N5253	0		13 37 05	-31 23 23	7061	6092.66	150	240	360	45.97	11.52	1.479	1.099	0.925	0.451	
N5353	-3		13 51 21	+40 31 30	3932	3217.63	150	420	540	72.89	11.80	0.518	0.198	1.005	0.440	
N5506	1	a	14 10 38	-02 58 30	c					3943.86	73.79	2.936	0.393	4.159	0.213	
N5548	1	a	14 15 43	+25 22 00	356	22397.22	600	1000	1200	24050.98	183.61	0.597	0.011	1.324	0.026	
N5683	0	a	14 33 06	+48 52 54	2625	2113.88	240	500	600	300.48	19.27	1.059	0.177	1.298	0.193	
N5838	-2		15 02 54	+02 17 36	10456	16108.10	120	420	540	107.45	15.77	0.358	0.128	0.791	0.410	
N5846	-2		15 03 56	+01 47 47	9975	14344.00	600	630	720	2498.25	127.81	0.907	0.102	0.710	0.093	
N6744	4		19 05 02	-63 56 17	7063	20546.09	240	420	540	423.17	39.29	1.724	0.583	1.251	0.213	
N6814	4	a	19 39 55	-10 26 36	354	26650.09	480	700	850	1548.02	85.51	1.411	0.270	1.685	0.188	
N6872	3		20 11 40	-70 55 30	1858	6609.35	270	360	480	162.27	28.47	0.443	0.188	1.171	0.618	
N6876	-5		20 13 05	-71 01 00	1858	6609.35	240	360	480	200.82	24.88	0.762	0.218	0.925	0.294	
N6946	5		20 33 48	+59 59 00	c					1985.77	116.48	1.378	0.302	1.523	0.171	
N7213	1	a	22 06 12	-47 25 00	6714	1648.81	600	700	800	4404.06	76.33	0.647	0.028	1.232	0.055	
N7320	7		22 33 45	+33 41 24	7827	2879.70	270	300	420	73.16	16.27	0.151	0.134	0.985	1.308	
I1459	-5		22 54 23	-36 43 47	6674	3277.35	240	330	450	124.47	16.89	1.425	0.588	1.208	0.319	
N7469	2	a	23 00 44	+08 36 17	c					3844.31	86.07	1.143	0.072	1.230	0.058	
N7552	4		23 13 25	-42 51 30	c					98.22	14.43	0.956	0.339	0.748	0.275	
N7582	2	a	23 15 38	-42 38 42	c					482.44	35.21	1.097	0.303	2.431	0.476	
N7590	5		23 16 11	-42 30 42	6385	9767.76	210	240	360	93.18	19.65	0.740	0.340	0.783	0.425	d
N7619	-5		23 17 43	+07 56 00	2598	8756.98	300	600	800	429.03	36.56	1.031	0.192	0.470	0.112	d
N7626	-5		23 18 10	+07 56 35	2598	8756.98	240	360	480	166.16	29.84	1.675	0.913	0.759	0.265	d

TABLE 4—*Continued*

Name	Type (T)	RA (1950) (h m s)	Dec (1950) (d ' ")	Seq	Exp. (sec)	Source radius (")	background radii (")		Counts	Error	C21	Error	C32	Error
N7673	5	23 25 12	+23 18 54	10201	4498.60	150	240	360	34.17	9.98	0.653	0.577	2.412	1.697
N7771	1 [a]	23 48 52	+19 50 00	6367	5642.00	210	300	400	103.19	17.66	0.665	0.295	1.411	0.577
N7793	7	23 55 15	-32 52 05	2146	1849.70	150	400	500	41.50	8.04	1.537	0.825	0.984	0.410

[a] AGN.
[b] X-ray emission may be contaminated by the intracluster emission.
[c] Merged (more than one observation, see table 5).
[d] Due to vignetting, C32 may be underestimated (see text).

(*open circles*) are near the 1 keV line. The acceptable temperature ranges are 0.5–1.5 keV for NGC 4636 (which is at the lowest point in C32) and 1–2 keV for the other three ellipticals (see Fig. 2 in § 2). Spiral galaxies (*filled circles*) have higher C32 than elliptical galaxies. The temperature ranges are 3–4 keV for NGC 4579 and open-ended toward a high temperature for NGC 2403, NGC 3628, and NGC 4594 (see Fig. 3).

In Figure 9*b*, we plot the sample of AGNs for which the X-ray emission is dominated by the central point source (see § 2.3). Again each galaxy is labeled by its name and the galaxy-by-galaxy comparison with the results in § 2 and KUC proves consistency between the standard fitting and the X-ray colors. Open circles identify objects with hydrogen column density lower than the Galactic values and filled circles identify the opposite extremes with N_H larger than the Galactic value (see Fig. 4 and KUC). NGC 4151 (which may contain a very soft emission component and cannot be fitted with a single component model) is outside the lines with $\alpha = 1$ and 2. Also plotted is NGC 1068 (denoted by asterisk), which has the steepest X-ray spectrum in our sample (and KUC).

We have derived X-ray colors for all the galaxies listed in Paper I with net counts larger than 30. Source count extraction is the same as in § 2.1. Some of the galaxies for which we have derived X-ray colors are in the periphery of the IPC field of view. The colors of these galaxies may be affected by a energy-dependent decrease of the effective area as a function of off-axis distance due to the telescope vignetting. We find that this effect is similar at 0.28 keV (C) and at 1.49 keV (Al) within 30′ from the detector center. Therefore the X-ray color C21 is basically not affected by vignetting. However at 3 keV (Ag) the effective area decreases more rapidly (Fabricant & Gorenstein 1979, SAO Internal Memorandum). This means that C32 is affected by vignetting in the sense that applying a vignetting correction would increase C32 for off-axis sources. We found that 12 galaxies would be affected and we marked these galaxies in Tables 4 and 5. In all cases, we have applied an average vignetting correction (with 1.5 keV values) to estimate total counts (see Harnden et al. 1984).

In Table 4, we list the galaxy name, morphological types, R.A. and Decl. (1950), observation sequences, exposure times, source and background radii, net counts and statistical errors, and X-ray colors and errors for 127 galaxies. For 29 galaxies observed more than once, we have combined counts and X-ray colors. These are marked in Table 4 and individual observations are listed in Table 5. We omit from Table 4 and Table 5 observations for which the X-ray color is unreasonable (negative counts in one band or very large error, greater than 100%). Most of these sources have small net counts so that small background fluctuation (by nearby sources, extended emission, etc.) might cause this failure. We will use these X-ray colors in Paper III to explore systematic spectral difference between different types of galaxies.

4. NOTES ON INDIVIDUAL GALAXIES

NGC 224.—M31 (Fabbiano et al. 1987; Trinchieri & Fabbiano 1991).

NGC 253.—Starburst galaxy (Fabbiano 1988b).

NGC 499 and NGC 507.—The Pisces cluster. The X-ray images of the two galaxies merge into each other. This region may have an extended cluster emission. The 99% range of H I column density for NGC 507 is larger than the Galactic N_H (in all models). The quantity kT (without considering N_H as a variable) is also given by Jones, Sullivan, & Bothun (1992).

NGC 598.—M33 (Trinchieri, Fabbiano, & Peres 1988).

NGC 985.—The 99% range of H I column density is lower than the Galactic N_H (in all models).

NGC 1068.—3C 71, M77, Arp 37; The power law slope (from two observations, IPC sequence 1927 and 1928) is the highest in the sample ($\alpha \sim 3$).

NGC 1097.—Arp 77; Gain (IPC sequence 2093) changed from 19.0 (for 317 s) to 12.2 (for 4998 s).

NGC 1218.—UGC 2555, 3C 78.

NGC 1313.—VV 436; The 99% range of H I column density is larger than the Galactic N_H (in all models). (Fabbiano & Trinchieri 1987).

NGC 1316.—Arp 154, For A.

NGC 1365.—VV 825.

NGC 1399 and NGC 1404.—(Killeen & Bicknell 1988). There may be extended emission from intracluster medium.

NGC 1566.—Between two observations (IPC sequence 1937 and 1938) the X-ray flux varies (Paper I), but the spectral properties are consistent with each other.

NGC 1569.—Arp 210.

NGC 1672.—VV 826 (Fabbiano & Trinchieri 1987).

NGC 1961.—Arp 184.

NGC 2403.—(Fabbiano & Trinchieri 1987).

NGC 2992.—Arp 245; Among three observations (IPC sequence 3060, 3061, and 6376) the X-ray flux varies (Paper I), but the spectral properties are consistent with each other. The 99% range of H I column density (IPC sequence 6376—longest observation) is larger than the Galactic N_H (in all models).

NGC 3031.—M81 (Fabbiano 1988a). The 99% range of H I column density is larger than the Galactic N_H in fits to brems-

TABLE 5

MULTIPLE OBSERVATIONS

Name	Seq	Exp. (sec)	Source radius (")	background radii (")		Counts	Error	C21	Error	C32	Error	
N0315	463	2022.99	150	360	450	38.64	8.00	0.806	0.429	1.398	0.681	
N0315	4374	17433.80	300	360	480	601.35	40.29	1.139	0.203	1.231	0.178	
N0936	5118	6421.19	330	360	480	104.11	29.52	1.562	1.645	1.597	0.852	
N0936	5771	5632.25	300	330	420	66.89	23.11	0.674	0.449	0.559	0.655	
N1068	1927	1456.43	360	420	540	783.22	31.14	0.360	0.035	0.716	0.102	
N1068	1928	2488.90	360	420	540	1396.53	41.14	0.559	0.038	0.745	0.064	
N1316	1883	3311.06	450	540	660	257.88	29.86	0.731	0.189	0.870	0.253	
N1316	1884	4840.88	450	540	660	368.11	35.51	0.497	0.100	0.556	0.210	
N1316	10571	3855.32	450	540	660	251.04	36.29	0.505	0.166	0.816	0.346	
N1365	3058	772.23	240	360	480	45.61	8.35	1.101	0.542	1.347	0.570	
N1365	3059	2921.63	330	360	480	160.41	22.52	0.496	0.172	1.170	0.442	
N1398	2096	8481.72	150	360	480	96.73	14.40	0.697	0.223	0.690	0.291	
N1398	2097	5331.02	210	360	480	78.23	14.74	0.334	0.162	1.291	0.753	
N1566	1937	2603.10	300	450	540	772.85	30.93	0.623	0.060	1.129	0.119	
N1566	1938	2529.00	300	450	540	488.74	26.41	0.733	0.101	1.328	0.169	
N2403	589	5988.29	390	420	540	294.53	32.75	0.759	0.217	1.542	0.400	
N2403	5226	4411.70	390	420	540	277.86	38.10	0.738	0.347	2.730	0.969	a
N2992	3060	1462.39	240	420	540	382.62	21.54	1.865	0.364	1.880	0.232	
N2992	3061	1526.85	270	420	540	375.99	21.31	1.779	0.363	2.368	0.306	
N2992	6376	7704.86	420	540	660	4659.45	77.17	2.636	0.198	2.371	0.087	
N3227	1945	2165.87	360	420	600	327.30	22.64	1.988	0.612	2.449	0.377	
N3227	1946	2310.05	360	420	600	1467.54	41.77	1.217	0.098	1.589	0.103	
N3227	7793	1462.40	240	300	420	580.14	34.26	1.129	0.205	2.269	0.320	a
N3516	1947	3948.26	300	500	700	604.28	29.76	0.929	0.138	2.107	0.247	
N3516	1948	3105.42	300	500	700	126.96	18.34	0.918	0.346	1.356	0.428	
N4038	469	1740.00	270	420	540	83.84	12.62	0.771	0.307	1.471	0.533	
N4038	7054	5213.25	210	420	540	179.59	17.92	0.886	0.207	0.855	0.204	
N4151	352	6901.04	360	720	820	1912.24	49.88	0.692	0.052	2.191	0.144	
N4151	353	19928.48	360	720	820	5522.28	84.20	0.699	0.030	2.189	0.085	
N4156	352	6901.04	180	720	820	78.92	14.54	1.042	0.496	1.109	0.441	
N4156	353	19928.48	180	720	820	325.81	26.03	0.592	0.128	1.845	0.376	
N4261	2672	2148.83	330	360	480	116.79	21.41	0.479	0.294	2.925	1.569	
N4261	6309	6905.93	330	360	480	326.35	36.57	0.841	0.219	0.833	0.228	
N4303	3267	1375.52	210	300	420	44.91	11.32	0.635	0.320	0.396	0.365	a
N4303	6986	10425.58	210	300	420	299.38	26.52	0.531	0.108	0.966	0.221	
N4365	6992	4854.00	120	360	480	50.62	9.95	1.191	0.657	1.201	0.501	
N4365	6993	4753.60	150	360	480	65.19	11.82	0.800	0.324	0.683	0.318	
N4374	278	34963.81	300	330	420	2781.68	122.80	0.826	0.085	1.045	0.113	a
N4374	4311	4558.25	300	330	450	300.30	40.05	1.159	0.429	1.227	0.362	a
N4382	2121	8148.04	300	360	480	175.16	28.86	0.516	0.185	0.779	0.382	
N4382	6994	10361.51	240	360	480	250.30	26.46	0.412	0.125	1.883	0.569	
N4477	281	14694.98	270	280	350	268.59	54.76	0.565	0.253	0.729	0.484	
N4477	2124	4388.06	210	240	360	120.65	25.38	1.039	0.406	0.137	0.226	a
N4477	7003	5068.47	150	210	330	96.86	16.98	0.684	0.250	0.562	0.316	a
N4579	2126	1058.81	270	360	480	241.67	18.17	1.262	0.243	1.064	0.183	
N4579	4315	7290.04	270	420	600	1591.79	45.62	1.069	0.078	1.148	0.077	
N4594	2127	5282.17	390	500	600	428.00	34.22	1.266	0.278	1.089	0.180	
N4594	2128	1207.36	390	500	600	141.93	18.69	0.853	0.302	1.463	0.438	
N4639	7013	5145.10	270	330	450	186.33	26.07	1.697	0.770	1.025	0.273	
N4639	7014	4430.59	270	330	450	162.67	23.26	0.513	0.180	1.243	0.464	

TABLE 5—*Continued*

Name	Seq	Exp. (sec)	Source radius (")	background radii (")		Counts	Error	C21	Error	C32	Error	
N4697	2134	4957.41	240	360	480	107.78	18.80	0.581	0.216	0.807	0.398	
N4697	4004	3484.64	300	360	480	71.55	22.64	0.807	0.565	0.867	0.695	a
N5506	3062	2257.06	360	550	750	527.50	27.31	2.033	0.586	4.150	0.575	
N5506	3063	1901.40	360	650	750	629.85	29.21	3.398	0.977	2.890	0.305	
N5506	7204	6454.32	360	400	600	1887.89	50.99	3.190	0.625	3.971	0.270	
N5506	9502	2942.27	360	400	600	898.62	35.29	2.609	0.819	5.447	0.625	
N6946	422	4879.50	480	600	700	251.86	44.06	1.264	0.597	0.987	0.356	
N6946	10314	20871.68	480	600	700	1301.77	90.04	1.264	0.302	1.669	0.226	
N6946	10597	7444.09	480	600	700	432.14	59.32	1.786	0.986	1.397	0.337	
N7469	1977	1938.56	750	760	900	1715.15	56.70	1.293	0.123	1.282	0.089	
N7469	1978	1990.98	720	760	900	2129.16	64.75	1.023	0.083	1.189	0.076	
N7552	5259	2056.48	180	400	500	52.80	10.56	1.163	0.552	0.603	0.288	
N7552	7582	1651.61	180	400	500	45.42	9.83	0.716	0.353	0.917	0.491	a
N7582	3066	1528.20	210	330	450	94.03	11.50	1.403	0.608	2.255	0.611	
N7582	3067	2106.14	240	330	450	109.11	13.99	1.367	1.037	5.126	1.841	
N7582	6385	9767.76	180	240	360	279.30	30.20	0.889	0.259	1.438	0.343	a

[a] Due to vignetting, C32 may be underestimated (see text).

strahlung and power-law model but consistent in a fit to thermal model. This galaxy has strong nuclear emission (see Fabbiano 1988a).

NGC 3034.—M82, Arp 337, 3C 231; starburst galaxy (Fabbiano 1988b). The 99% range of H I column density is larger than the Galactic N_H (in all models).

NGC 3227.—Arp 94, VV 209; The X-ray centroid coincides with NGC 3227, but NGC 3226 is inside the X-ray emission (see Paper I). Among three observations (IPC sequence 1945, 1946, and 7793) the X-ray flux varies, but the spectral properties are consistent with each other. The 99% range of H I column density (IPC sequence 1946—longest observation) is larger than the Galactic N_H (in all models).

NGC 3310.—Arp 217.

NGC 3395.—Arp 270, VV 246; The X-ray centroid coincides with NGC 3395. But NGC 3396 could contribute to the X-ray emission.

NGC 3516.—Variable X-ray flux (see Paper I).

NGC 3607.—Nearby X-ray sources (see Paper I).

NGC 3628.—Arp 317, VV 308; Starburst galaxy (Fabbiano et al. 1990). The 99% range of H I column density is larger than the Galactic N_H in fits to bremsstrahlung and thermal models, but consistent in a fit with power law.

N3660.—Mkn 1291.

NGC 4038.—N4038 + N4039 Antennae, VV 245, Arp 244; The two galaxies (NGC 4038 and NGC 4039) are not resolved in X-rays.

NGC 4051.—Gain (IPC sequence 7200) changed from 15.6 (for 2652 s), to 19 (for 4124 s) and to 12.5 (for 1580 s). The 99% range of H I column density is lower than the Galactic N_H (in all models).

NGC 4151.—Gain (IPC sequence 353) changed from 15.6 (for 1053 s), to 18 (for 9006 s) and to 12.8 (for 9870 s). The 99% range of H I column density (in both IPC sequence 352, 353) is lower than the Galactic N_H (in all models). The fit to a single component (in both observations) is bad. There may be an additional soft component.

NGC 4192.—M98.

NGC 4254.—M99.

NGC 4261.—3C 270.

NGC 4291.—Nearby X-ray source, Mkn 205 (see Paper I). The 99% range of N_H is larger than the Galactic N_H in a fit to Raymond thermal model, but consistent in fits to bremsstrahlung and power law.

NGC 4298.—The two galaxies (NGC 4298 and NGC 4302) are barely resolved. The X-ray emission is treated as one source.

NGC 4303.—M61.

NGC 4321.—M100.

NGC 4374.—M84, 3C 272.1.

NGC 4382.—M85.

NGC 4406.—M86.

NGC 4472.—M49, Arp 134; gain (IPC sequence 4308) changed from 18.1 (for 1715 s), to 14 (for 5957 s).

NGC 4501.—M88.

NGC 4552.—M89.

NGC 4567.—The two galaxies (NGC 4567 and NGC 4568) are barely resolved. The X-ray emission is treated as one source.

NGC 4579.—M58. The 99% range of H I column density is larger than the Galactic N_H (in all models).

NGC 4594.—Sombrero, M104.

NGC 4631.—Arp 281.

NGC 4649.—M60, VV 206, Arp 116.

NGC 4756.—Gain (IPC sequence 1900) changed from 23.3 (for 1611 s), to 15.5 (for 3900 s).

NGC 4826.—M64.

NGC 4861.—Mkn 59, Arp 266.

NGC 5128.—Cen A, Arp 153.

NGC 5236.—M83.

NGC 5353.—The two galaxies (NGC 5353 and NGC 5354) are not resolved, but the X-ray centroid is close to NGC 5353 (see also the HRI image in Paper I).

NGC 5506.—Mkn 1376; The 99% range of H I column density (in all four sequences) is larger than the Galactic N_H (in all models).

NGC 5236.—Gain (IPC sequence 588) changed from 19 (for 1622 s), to 12.2 (for 4086 s).

NGC 5457.—M101 (Trinchieri et al. 1990).

NGC 5548.—Mkn 9027; The 99% range of H I column density is lower than the Galactic N_H (in all models).

NGC 5683.—Mkn 474.

NGC 6872.—VV297.

NGC 6946.—Arp29.

NGC 7320.—The three nearby galaxies (NGC 7320, 7317, and 7319) are not resolved.

NGC 7469.—Arp298; The 99% range of H I column density is larger than the Galactic N_H (in all models).

NGC 7619.—Nearby X-ray source, NGC 7626 (see Paper I).

NGC 7673.—Mkn 325.

NGC 7771.—Mkn 9006.

5. SUMMARY

We have presented spectral parameters for 43 galaxies and X-ray colors for 127 galaxies using the *Einstein* IPC data. The emission temperature of elliptical galaxies is approximately 1–2 keV and the temperature ranges of spiral galaxies are usually open-ended toward higher temperatures (beyond 5 keV). However, there are galaxies which do not follow this general rule. In particular, NGC 507 has a higher temperature than typical for early-type galaxies and M81 has a lower temperature than typical for late-type galaxies. The N_H fitted from the X-ray spectra is generally in agreement with the line-of-sight Galactic H I column density in both early- and late-type galaxies. There are, however, exceptions in both types of galaxies and they generally are in the sense of suggesting an increase of absorption within the galaxies. In spiral galaxies large intrinsic N_H are present within two galaxies with small active (or possible active) nuclei, M81 and NGC 1313, and in galaxies with a dusty starburst nucleus, M82 and NGC 3628. More puzzling is the presence of large intrinsic N_H in some early-type galaxies. We present the results of fits to absorbed power laws for six AGNs. These are either not included in the sample of KUC, or we have obtained different results. For four AGNs the acceptable range of hydrogen column density is smaller than the Galactic value. This may suggest an extra soft component in these systems as suggested by KUC.

We have introduced X-ray colors to estimate spectral properties of weak X-ray sources. These X-ray colors are consistent with the results of the standard model fitting technique. The X-ray colors of 127 galaxies have been presented in this paper and will be used to determine systematic X-ray properties of different classes of galaxies in a forthcoming paper (Paper III).

We thank Susan Hazelton, Elizabeth Bohlen, Linda Kim, Chris Fassnacht, and Archan Basu for help in the data analysis and Claude Canizares, Patrick Slane, and Harvey Tananbaum for comments on the manuscript. This work was supported by NASA grant NAG5-1202, NASA contract NAS8-30751 and Smithsonian Institution Scholarly Studies grant S910. G.T. acknowledges financial support by Italian ASI.

REFERENCES

Avni, Y. 1976, ApJ, 210, 642
Brown, R. L., & Gould, R. J. 1970, Phys. Rev. D, 1, 2252
Cordova, F. A., Kartje, J., Mason, K. O., & Mittaz, J. P. D. 1990, in Imaging X-ray Astronomy, ed. E. Elvis (Cambridge: Cambridge Univ. Press), 273
de Vaucouleurs, G., de Vaucouleurs, A., & Corwin, H. 1976, Second Reference Catalogue of Bright Galaxies (Austin: Univ. of Texas) (RC2)
Fabbiano, G. 1988a, ApJ, 325, 544
———. 1988b, ApJ, 330, 672
———. 1989, ARA&A, 27, 87
Fabbiano, G., Heckman, T., & Keel, W. C. 1990, ApJ, 355, 442
Fabbiano, G., Kim, D.-W., & Trinchieri, G. 1992, ApJS, 80, 531 (Paper I)
Fabbiano, G., & Trinchieri, G. 1987, ApJ, 315, 46
Fabbiano, G., Trinchieri, G., & Van Speybroeck, L. S. 1987, ApJ, 316, 127
Filippenko, A. V., & Sargent, W. L. W. 1985, ApJS, 57, 503
Forman, W., Jones, C., & Tucker, W. H. 1985, ApJ, 293, 102
Giacconi, R., et al. 1979, ApJ, 230, 540
Harnden, F. R., Jr., Fabricant, D., Harris, D., & Schwartz, J. 1984, Smithsonian Astrophys. Obs. Spec. Rep., 393
Harris, D. H. 1984, *Einstein* Observatory Revised User's Manual (SAO internal publication)
Jones, C., Sullivan, W., & Bothun, G. 1992, AJ, submitted
Killeen, N. E. B., & Bicknell, G. V. 1988, ApJ, 325, 165
Kim, D.-W., Fabbiano, G., & Eskridge, P. 1992, in preparation
Kim, D.-W., Fabbiano, G., & Trinchieri, G. 1992, ApJ, in press (Paper III)
Kruper, J. S., Urry, C. M., & Canizares, C. R. 1990, ApJS, 74, 347 (KUC)
Pounds, K. A., Warwick, R. S., Culhane, J. L., & deKorte, P. A. J. 1986, MNRAS, 218, 685
Sandage, A. R., & Tammann, G. A. 1981, Revised Shapley-Ames Catalogue of Galaxies (Washington, DC: Carnegie Institute) (RSA)
Schweizer, F. 1987, in IAU Symp. 127, Structure and Dynamics of Elliptical Galaxies, ed. T. deZeeuw (Dordrecht: Kluwer), 109
Stark, A. A., Heiles, C., Bally, J., & Linke, R. 1992, submitted
Trinchieri, G., & Fabbiano, G. 1991, ApJ, 382, 82
Trinchieri, G., Fabbiano, G., & Canizares, C. R. 1986, ApJ, 310, 637
Trinchieri, G., Fabbiano, G., & Peres, G. 1988, ApJ, 325, 531
Trinchieri, G., Fabbiano, G., & Romaine, S. 1990, ApJ, 356, 110
Wilkes, B. J., & Elvis, M. 1987, ApJ, 323, 243